Linking the formation and fate of exo-Kuiper belts within Solar system analogues

Dimitri Veras, Katja Reichert, Francesco Flammini dotti, Maxwell Cai, Alexander Mustill, Andrew Shannon, Catriona Mcdonald, Simon Portegies zwart, M Kouwenhoven, Rainer Spurzem

Monthly Notices
of the
ROYAL ASTRONOMICAL SOCIETY

MNRAS **493,** 5062–5078 (2020)
Advance Access publication 2020 March 3

doi:10.1093/mnras/staa559

Linking the formation and fate of exo-Kuiper belts within Solar system analogues

Dimitri Veras [1,2]★† Katja Reichert,[3] Francesco Flammini Dotti [4,5] Maxwell X. Cai [6,7] Alexander J. Mustill [8] Andrew Shannon,[9] Catriona H. McDonald [1,2] Simon Portegies Zwart,[7] M. B. N. Kouwenhoven[4] and Rainer Spurzem[3,10,11]‡

[1]*Centre for Exoplanets and Habitability, University of Warwick, Coventry CV4 7AL, UK*
[2]*Department of Physics, University of Warwick, Coventry CV4 7AL, UK*
[3]*Astronomisches Rechen-Institut, Zentrum für Astronomie der Universität Heidelberg, Mönchhofstr 12-14, D-69120 Heidelberg, Germany*
[4]*Department of Physics, School of Science, Xi'an Jiaotong-Liverpool University, 111 Ren'ai Rd., Suzhou Dushu Lake Science and Education Innovation District, Suzhou Industrial Park, Suzhou 215123, China*
[5]*Department of Mathematical Sciences, University of Liverpool, Liverpool L69 3BX, UK*
[6]*SURFsara, Science Park 140, NL-1098 XG Amsterdam, the Netherlands*
[7]*Leiden Observatory, Leiden University, PO Box 9513, RA Leiden NL-2300, the Netherlands*
[8]*Lund Observatory, Department of Astronomy & Theoretical Physics, Lund University, Box 43, SE-221 00 Lund, Sweden*
[9]*LESIA, Observatoire de Paris, Université PSL, CNRS, Sorbonne Université, Université de Paris, 5 place Jules Janssen, F-92195 Meudon, France*
[10]*National Astronomical Observatories and Key Laboratory of Computational Astrophysics, Chinese Academy of Sciences, 20A Datun Rd., Chaoyang District, Beijing 100101, China*
[11]*Kavli Institute for Astronomy and Astrophysics, Peking University, Yiheyuan Lu 5, Haidian Qu, Beijing 100871, China*

Accepted 2020 February 19. Received 2020 February 19; in original form 2019 November 28

ABSTRACT

Escalating observations of exo-minor planets and their destroyed remnants both passing through the Solar system and within white dwarf planetary systems motivate an understanding of the orbital history and fate of exo-Kuiper belts and planetesimal discs. Here, we explore how the structure of a 40–1000 au annulus of planetesimals orbiting inside of a Solar system analogue that is itself initially embedded within a stellar cluster environment varies as the star evolves through all of its stellar phases. We attempt this computationally challenging link in four parts: (1) by performing stellar cluster simulations lasting 100 Myr, (2) by making assumptions about the subsequent quiescent 11 Gyr main-sequence evolution, (3) by performing simulations throughout the giant branch phases of evolution, and (4) by making assumptions about the belt's evolution during the white dwarf phase. Throughout these stages, we estimate the planetesimals' gravitational responses to analogues of the four Solar system giant planets, as well as to collisional grinding, Galactic tides, stellar flybys, and stellar radiation. We find that the imprint of stellar cluster dynamics on the architecture of $\gtrsim$100 km-sized exo-Kuiper belt planetesimals is retained throughout all phases of stellar evolution unless violent gravitational instabilities are triggered either (1) amongst the giant planets, or (2) due to a close ($\ll 10^3$ au) stellar flyby. In the absence of these instabilities, these minor planets simply double their semimajor axis while retaining their primordial post-cluster eccentricity and inclination distributions, with implications for the free-floating planetesimal population and metal-polluted white dwarfs.

Key words: Kuiper belt: general – minor planets, asteroids: general – planets and satellites: dynamical evolution and stability – stars: evolution – stars: formation – white dwarfs.

1 INTRODUCTION

The Kuiper belt and scattered disc refer to the collection of minor planets, which orbit the Sun at separations between tens

★ E-mail: d.veras@warwick.ac.uk
† STFC Ernest Rutherford Fellow.
‡ Research Fellow of Frankfurt Institute for Advanced Studies.

and hundreds of astronomical units. These objects provide crucial constraints on the temporal evolution of the Solar system. With respect to formation, the *New Horizons* mission has revolutionized our understanding of Pluto's geophysical history (Stern et al. 2015; Moore et al. 2016) as well as the formation pathway of the 'squashed snowman' binary object 486958 Arrokoth (2014 MU69 Ultima Thule) (Nesvorný et al. 2019; Stern et al. 2019). Alternatively, with respect to the fate of Kuiper belt and scattered disc objects, we must look towards the interstellar interlopers or *sōlus lapis* 1I/'Oumuamua (Meech et al. 2017; Williams 2017) and 2I/Borisov (Guzik et al. 2019) or elsewhere, in evolved extrasolar planetary systems (Portegies Zwart et al. 2018).

Besides the Sun, the only other stars around which the presence of individual minor planets have been observed or inferred are young hot stars – where variable absorption is inferred to come from gas (Ferlet, Hobbs & Madjar 1987; Welsh & Montgomery 2015) and possibly dust (Rappaport et al. 2018) released by individual comets – and white dwarfs (Vanderburg et al. 2015; Manser et al. 2019; Vanderbosch et al. 2019), which represent the endpoint of stellar evolution for nearly all Milky Way stars. The destroyed remnants of other minor planets are observed through the presence of over 40 debris discs around white dwarfs (e.g. Zuckerman & Becklin 1987; Graham et al. 1990; Gänsicke et al. 2006; Farihi 2016; Dennihy et al. 2018; Swan, Farihi & Wilson 2019a) and the constituents of over 1000 minor planets are observed inside the atmospheres of white dwarfs (Zuckerman et al. 2003, 2010; Koester, Gänsicke & Farihi 2014; Coutu et al. 2019). This minor planet destruction provides a unique means to probe the bulk composition of asteroids and comets beyond our Solar system.

Consequently, linking the formation and fate of minor planets has importance in multiple astrophysical contexts. However, the computationally challenging nature of this task has motivated investigations that focus on a single or a few phases of stellar evolution. For example, the dynamical origin of the currently observed Kuiper belt architecture has been the subject of numerous investigations (e.g. Gomes et al. 2008; Liou & Kaufmann 2008; Punzo, Capuzzo-Dolcetta & Portegies Zwart 2014; Nesvorný 2018) that are almost entirely restricted to the early main-sequence phase of the Sun, or have considered just the post-formation evolution (e.g. Tiscareno & Malhotra 2009; Lawler et al. 2017; Shannon & Dawson 2018). Other theoretical studies dedicated to minor planets are focused solely on the white dwarf phase (e.g. Alcock, Fristrom & Siegelman 1986; Wyatt et al. 2014; Stone, Metzger & Loeb 2015; Veras, Eggl & Gänsicke 2015a; Veras, Marsh & Gänsicke 2016a; Brown, Veras & Gänsicke 2017; Grishin & Veras 2019; Makarov & Veras 2019), and sometimes on individual systems (Gurri, Veras & Gänsicke 2017; Veras et al. 2017a; Duvvuri, Redfield & Veras 2019; Veras, McDonald & Makarov 2020a).

Between the main-sequence and white dwarf phases of stellar evolution, most stars experience violent physical alterations during the giant branch phases. Minor planets are particularly susceptible to these changes (Veras 2016a) and the consequences have again represented the focus of investigations during this phase alone. These changes include radiative destruction due to YORP-induced rotational fission (Veras, Jacobson & Gänsicke 2014a; Veras & Scheeres 2020) – potentially contributing to the formation of debris discs (Bonsor & Wyatt 2010; Bonsor et al. 2013, 2014) – and orbital evolution due to both the Yarkovsky effect (Veras, Eggl & Gänsicke 2015b; Veras, Higuchi & Ida 2019) and stellar mass-loss (Omarov 1962; Hadjidemetriou 1963). In particular, stellar mass-loss can eject these minor planets (Veras et al. 2011), which may eventually pass through other planetary systems (Do, Tucker & Tonry 2018; Moro-Martín 2019).

Other investigations that included minor planet evolution have attempted to bridge the gap between several stellar evolutionary phases and/or included the influence of major planets (Bonsor, Mustill & Wyatt 2011; Debes, Walsh & Stark 2012; Frewen & Hansen 2014; Antoniadou & Veras 2016, 2019; Veras et al. 2016b; Caiazzo & Heyl 2017; Mustill et al. 2018; Smallwood et al. 2018, 2019) or binary stars (Bonsor & Veras 2015; Hamers & Portegies Zwart 2016; Petrovich & Muñoz 2017). None, however, have calibrated their minor planet initial conditions – which could sensitively determine the eventual accretion rate on to white dwarfs – with the results of planetary system formation within stellar clusters.

Nearly all planetary systems are formed in clustered stellar environments, with implications for planet formation (e.g. Grishin, Perets & Avni 2019). Hence, theoretical investigations of these systems are of paramount importance, despite detections of only a few dozen cluster planets (Brucalassi et al. 2017, Mann et al. 2017, Leão et al. 2018, and see table 1 of Cai et al. 2019 for an up-to-date listing of cluster planets). Many studies have focused on how photo-evaporation from young hot stars affects major planet formation and migration (Adams et al. 2004; Veras & Armitage 2004; Anderson, Adams & Calvet 2013; Dai et al. 2018; Winter et al. 2018; Concha-Ramírez et al. 2019; Nicholson et al. 2019) and how frequent and slow stellar flybys influence the resulting major planet architecture (Malmberg et al. 2007; Malmberg, Davies & Heggie 2011; Hao, Kouwenhoven & Spurzem 2013; Zheng, Kouwenhoven & Wang 2015; Shara, Hurley & Mardling 2016; Cai et al. 2017, 2019; Hamers & Tremaine 2017; Flammini Dotti et al. 2019; Li, Mustill & Davies 2019; van Elteren et al. 2019). Less-studied have been the consequences for minor planets (see e.g. Brasser, Duncan & Levison 2006; Pfalzner et al. 2018; Hands et al. 2019; Batygin et al. 2020).

Here, we attempt to qualitatively trace the evolution, across all stellar phases, of exo-Kuiper belts and planetesimal discs which are shaped in a stellar cluster environment. In order to restrict the enormous parameter space associated with this task, we consider only Solar system analogues (Sun-like stars with Jupiter, Saturn, Uranus, and Neptune) and split the temporal evolution into four distinct segments: (i) stellar cluster evolution (Section 2), (ii) main-sequence evolution (Section 3), (iii) giant branch evolution (Section 4), and (iv) white dwarf evolution (Section 5). A schematic overview of the different segments and the numerical codes used is given in Fig. 1. We discuss the results in Section 6 and conclude in Section 7.

2 STAR CLUSTER EVOLUTION

Star formation occurs in regions with a stellar density that is substantially higher than that of the Galactic neighbourhood. Consequently, within a cluster, close stellar flybys are frequent and slow; they can help sculpt the orbital distribution of objects which are sufficiently far from their parent stars. Modelling these interactions is challenging primarily because of the different time-scales (cluster evolution and planetary evolution) that must be simulated self-consistently, and secondarily because of the large parameter space.

In this section, we detail our cluster simulations. We describe our computational approach in Section 2.1 before outlining the initial conditions for our star clusters (Section 2.2) and planetary systems (Section 2.3); we report the simulation output in Section 2.4.

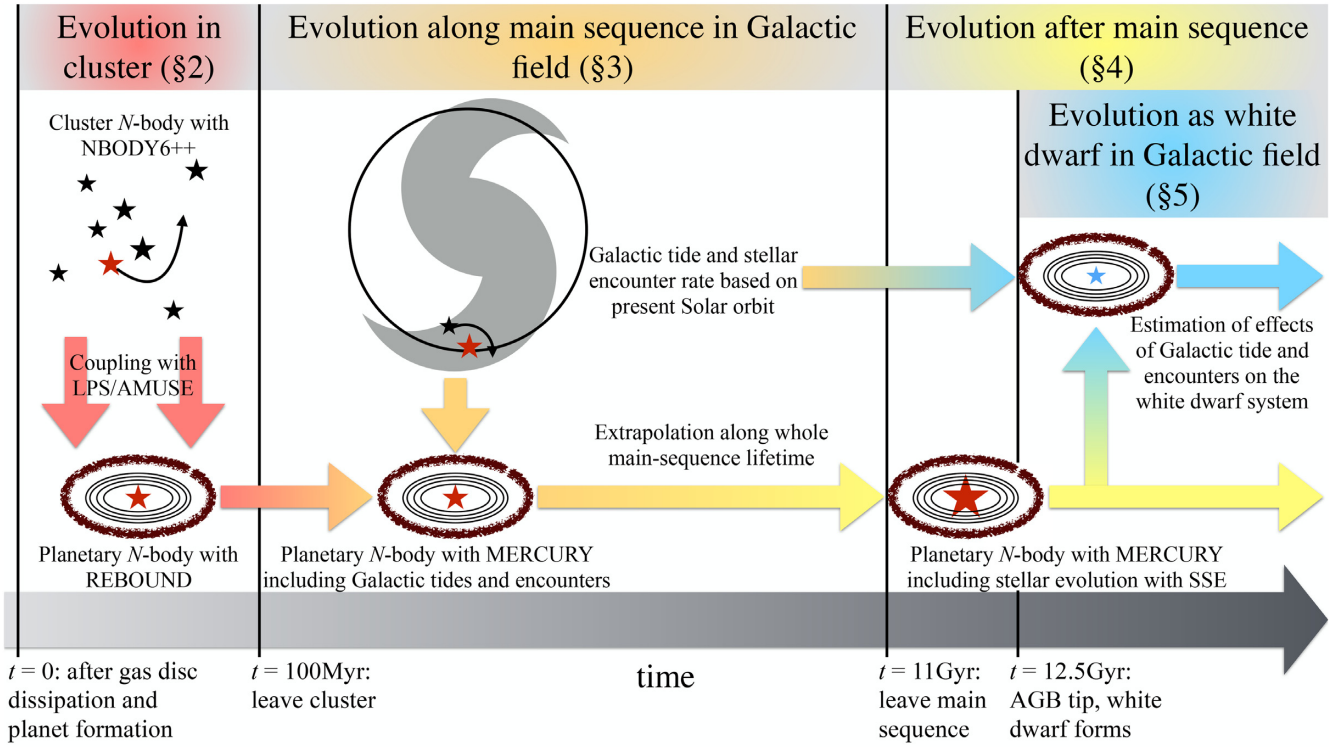

Figure 1. Overview of the evolution of our planetary systems and the numerical codes (in all caps) used to study each stage. In Section 2, we place a newly formed planetary system in a stellar cluster and follow its evolution for 100 Myr. We then take the resulting system configuration at 100 Myr – assumed to be the time at which the cluster dissolves – and integrate the planetary and planetesimal orbits under the effects of stellar and planetary gravity, Galactic tides, and encounters with stars in the field (Section 3). Because we find that the effects of tides and flybys are unimportant, and the system is inherently stable, we assume that the system configuration at the end of the main sequence – at 11 Gyr – remains unchanged from the configuration at 100 Myr. We then use this configuration as initial conditions for our post-main-sequence simulations, which feature red giant branch and asymptotic giant branch (AGB) mass-loss, followed by several Gyr of white dwarf cooling (Section 4). Finally, we also estimate the effects of the Galactic environment on the expanded systems orbiting white dwarfs (Section 5).

2.1 Computational approach

Planetary system evolution is fundamentally different from star cluster evolution. In the absence of major instabilities, planets evolve quiescently and are subject to only minor perturbations from mutual gravitational interactions and external perturbations from passing stars. The time-scale for orbital changes is typically secular.

Star clusters, on the other hand, evolve through two-body relaxation and close few-body encounters (which may involve close binaries). These processes produce changes on orbital time-scales rather than secular time-scales. Further, star cluster dynamics more readily exhibit deterministic chaos, where systems with slightly different initial conditions diverge from each other in phase space exponentially, in less than an orbital time (e.g. Miller 1964; Quinlan & Tremaine 1992).

For these reasons, executing a combined simulation of planetary systems in star clusters is challenging. The main obstacle to overcome is not actually establishing the different time-scales or hierarchies in the integrations,[1] but rather accurately modelling the resonant and secular effects in the internal evolution of planetary systems. While different authors have advocated special symplectic methods to model planetary systems accurately (e.g. Wisdom & Holman 1991), Kokubo, Yoshinaga & Makino (1998) demonstrated how small improvements in the Hermite integrator used for star cluster simulations can lead to an accurate treatment of its internal planetary systems over Gyr time-scales.

We previously successfully performed simulations involving star clusters and their internal planetary systems by using a single *N*-body code (NBODY6++GPU with massless particles, e.g. Shu et al., in preparation; Spurzem et al. 2009). In this work, we follow a different method, one used by Flammini Dotti et al. (2019) and Cai et al. (2017, 2019). Here we first integrate the star cluster dynamics, recording the trajectories of stars and their nearest neighbours. Then, we add in planetary systems (including the exo-Kuiper belt objects) to selected host stars; the evolution of these planetary systems is performed by another code, named LONELYPLANETS (Cai et al. 2017; Cai, Portegies Zwart & van Elteren 2018; Cai et al. 2019; Flammini Dotti et al. 2019, 2020). LONELYPLANETS utilizes the recorded perturbations from the star cluster simulation outputs as external perturbations to the planetary systems.

Hence, the star cluster simulations are carried out by NBODY6++GPU (Wang et al. 2015, 2016), whereas the planetary systems are integrated by LONELYPLANETS (hereafter, LPS). This approach represents a fast and accurate method for integrating the evolution of planetary systems in star clusters, under the condition that the force of the planets on the stellar population can be neglected. The star cluster evolution is integrated through the Hermite scheme, using NBODY6++GPU. This code is the latest updated version of the original NBODY6 (Aarseth 1999) and NBODY6++ (Spurzem 1999). The greatest improvement in the last

[1]Close stellar binaries and planetary systems can be treated similarly.

version is the feature that takes advantage of graphical processing units (GPUs) and task parallelization. The latter is achieved through MPI (Message Passing Interface; Tapamo 2009), where both regular and irregular forces are parallelized. The GPU usage significantly improves NBODY6++GPU performance, especially for long-range (regular) gravitational forces

LPS is based on the AMUSE framework (Portegies Zwart 2011; McMillan et al. 2012; Pelupessy et al. 2013; Portegies Zwart et al. 2018). AMUSE helps us consolidate our methodology, which can be summarized in four steps: (i) setting initial conditions for modelling the star cluster and planetary systems; (ii) modelling numerically the dynamics and stellar evolution of the star cluster; (iii) identifying close encounters experienced by the planet-hosting stars; and (iv) modelling the evolution of the planetary systems under the influence of the closest perturbers. In our work we will consider the five closest perturbers to the host stars, and these perturbers are identified by using the standard method for neighbour selection in the NBODY6++GPU simulations.

NBODY6++GPU integrates the star clusters, and stores data at a high temporal resolution (i.e. star cluster output) by using the block time-step scheme (BTS; Cai et al. 2015). The latter approach prevents data redundancy for planetary systems in the low temporal resolution regime (i.e. planetary output). These data are then sent to the REBOUND integrator (Rein & Liu 2012), which integrates the planetary system until the next BTS output set of data: in our data set the star cluster output time-step of ∼1000 yr was adopted. We use the HDF5[2] output format (Portell de Mora et al. 2011), a highly efficient storage scheme organized in a data base-like structure.

As the star cluster and the planetary systems evolve, escaping bodies are removed. The criterion for escape of a star in a stellar cluster in NBODY6++GPU is when $r > 2r_{\rm tid}$, where $r_{\rm tid}$ is the star cluster's tidal radius (see Section 2.2 for further information). In LPS, the escapers from the planetary system are those particles with orbital eccentricities $e > 0.995$.

2.2 Star cluster initial conditions

We place our planetary systems each within a stellar cluster of 2000 stars containing an initial total mass of 1139 $M_\odot$. The initial mass function (IMF) for the stars in the cluster follows a Kroupa (2001) IMF. The stellar masses are drawn from the range 0.08–100 $M_\odot$ with an expected average mass of 0.57 $M_\odot$. We use a Plummer (1911) model in virial equilibrium as the density profile for the cluster from which the initial positions and velocities of the stars are drawn. The initial half-mass radius $r_{\rm hm}$ is 0.73 pc while the initial central density is 896 $M_\odot\,{\rm pc}^{-3}$. These values are motivated from studies of the star cluster in which the Sun might have been born (Portegies Zwart 2009, 2019). Furthermore, we assume a standard solar neighbourhood tidal field (Heisler & Tremaine 1986) and no primordial mass segregation.

The fraction of primordial binary systems is set to 0 per cent in order to (i) keep the external perturbations 'clean' and associate external perturbations entirely with single stars and not three-body effects, (ii) avoid circumbinary planetary systems and potential exchange interactions, and (iii) maintain a reasonable computational cost for the simulations. In reality, observations indicate that the binary fraction varies from a few per cent to half, where the lower bound is more representative of globular clusters and the upper bound is more representative of the field (Geller et al. 2008; Raghavan et al. 2010; Milone et al. 2012). A binary flyby typically increases the cross-section for planetary ejection and collisions (Wang, Perna & Leigh 2020). Hence, including binary flybys would have likely increased the extent of destabilization of the disc, although the severity of the destabilization would have been dependent on multiple parameter choices.

[2]https://www.hdfgroup.org/

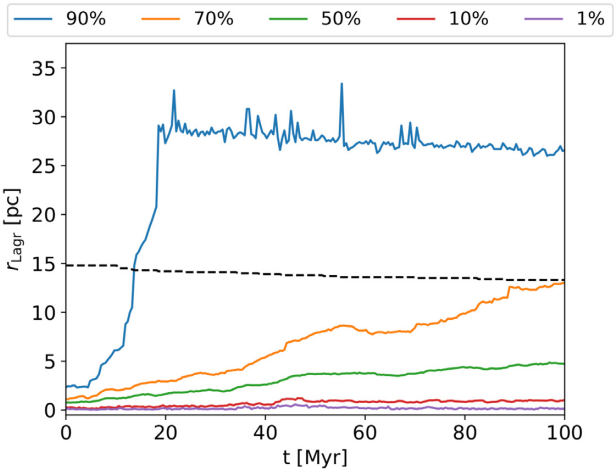

Figure 2. Lagrangian radii $r_{\rm Lagr}$ of the star cluster, containing the fraction of current total mass (from 1 to 90 per cent, from the bottom curve moving upwards; see legend on top of plot), as a function of time. For comparison, the tidal radius $r_{\rm tid}$ is shown by the black dashed line. See main text for further explanation.

NBODY6++GPU includes stellar evolution of single and binary stars according to Hurley, Pols & Tout (2000) and Hurley et al. (2001). We assume a solar metallicity for all stars, and include further improvements by taking into account fallback from supernova explosions and stellar winds of massive stars (Belczynski, Kalogera & Bulik 2002). Also, kicks occurring at the formation of neutron stars according to Hobbs et al. (2005) are included. Although stellar evolution is modelled in our cluster simulations, the effects of mass-loss of the host star on the planetary systems are not: the consequences for the major and minor planets during the main-sequence phase would be negligible for our 1 $M_\odot$ host stars.

We define a tidal radius $r_{\rm tid}$ as given in Cai et al. (2016). This radius is similar to the Jacobi radius $r_{\rm J}$ and is related to the quantity $r_{\rm lim}$ that was defined by King (1962) (see Ernst, Just & Spurzem 2009 for further discussion). The differences between these three quantities are small, of order unity. Our *N*-body simulation considers stars who reach twice the tidal radius as escapers and removes them from the system, meaning that some stars that are unbound from the cluster are followed. We do acknowledge, however, that the concept of a spherical tidal radius is an approximation; in reality the tidal escape problem is much more complicated (cf. e.g. Ernst, Just & Spurzem 2009). By keeping stars in the simulation which are not bound to the cluster, we can follow for the dynamics near the Lagrangian points with our *N*-body simulations in detail.

Fig. 2 provides an overview of the global evolution of our star cluster through the Lagrangian radii, which contain the indicated fraction of current total mass. Note that the 90 per cent Lagrangian radius stays approximately constant after it has reached twice the tidal radius, because at this point we start removing particles from the simulation. We have also plotted the tidal radius as a function of time in that figure. At the time where the tidal radius is equal to the half-mass radius (50 per cent Lagrangian radius), the mass-loss of the bound part of the star cluster is 50 per cent: this time

defines the half-life of the cluster. In this paper, we simulate the cluster environment of our planetary systems for 100 Myr because after this time the cluster is going to dissolve and will have reduced its central density significantly; most strong encounters will have occurred by 100 Myr.

2.3 Planetary system initial conditions

Now we turn to the planetary systems. We define $t = 0$ as the time when the natal protoplanetary disc has dissipated, and all that remains are major and minor planets, as well as the parent Sun-like star (with a mass of 1.0 $M_{\odot}$).

At this time, we emplace four major planets into an artificial system. The major planets are analogues of Jupiter, Saturn, Uranus, and Neptune in mass, radius, and current separation. As the protoplanetary disc lifetime was likely a few million years (Pascucci & Tachibana 2010; Williams & Cieza 2011), and (at least in the Sun's case) the protostar may form a few Myr after the first stars in the cluster (Adams 2010), the star may depart the cluster slightly earlier than is assumed here.

Besides circular, coplanar orbits, we assume currently observed planetary separations because the original orbital distribution of the four giant planets in our Solar system is unknown. The giant planets were likely in a more compact configuration in the past, and Neptune's outward migration explains resonant populations in the Kuiper belt (Malhotra 1993). On the other hand, a prior inwards migration of the giant planets can explain Jupiter's composition and the asymmetry of its Trojan populations (Öberg & Wordsworth 2019; Pirani et al. 2019). Additionally, the giant planets likely underwent at least one gravitational instability which has re-ordered the planets at some, still uncertain, previous epoch (Thommes, Duncan & Levison 2002; Tsiganis et al. 2005; Morbidelli et al. 2007; Nesvorný & Morbidelli 2012; Morbidelli et al. 2018). These instabilities have also shaped the Kuiper belt and scattered disc. Furthermore, the current configuration of the four giant planets in the Solar system is not expected to undergo any future instability amongst themselves (without an external influence) during the remainder of the Sun's main-sequence lifetime (Laskar & Gastineau 2009; Hayes, Malykh & Danforth 2010; Zeebe 2015; Veras 2016b).

This analogue Solar system serves as a template for our simulations. We generate 11 of these systems and impose different planetesimal disc configurations on each. We deposit 2000 massless particles in each planetesimal disc in an annulus extending from $a = 40$ to 1000 au, placing them uniformly in semimajor axis. Although these test particles are massless, we treat each as having a diameter of at least 100 km for the later application of radiative forces. The outer distance bound of 1000 au approximates the aphelion of distant Solar system objects such as 90377 Sedna. These particles feel the gravitational force of the star and planets, but do not exert a force. The particles, which will henceforth be denoted by planetesimals, are on initially circular and coplanar orbits with randomly distributed mean anomalies.

These discs are initially dynamically cold in order to ensure that subsequent changes to the eccentricity and inclination are not primordial, and can be interpreted entirely in terms of gravitational excitation by stars and major planets. These discs are similar to the broad planetesimal discs formed in the models of Carrera et al. (2017), where photoevaporation of a disc several hundred au wide drives efficient planetesimal formation by the streaming instability at large radii.

However, there is no observational confirmation that the models adopted in Carrera et al. (2017) are correct. Hence, because the disc is composed of test particles, we could divide the disc into different regions that may be treated independently. One natural dividing line is the maximum radial extent of observed debris discs. This value is debatable, particularly with respect to how they evolve out of protoplanetary discs (Andrews 2020), but we adopt a value of 150 au.

A value of 150 au appears to represent a reasonable upper limit given infrared observations of debris discs (Sibthorpe et al. 2018, and the catalogue of resolved debris discs by Pawellek and Krivov);[3] see also Krivov et al. (2013) with the caveat that some of these discs may actually be background galaxies (Gáspár & Rieke 2014). However, we caution that non-detectability does not necessarily translate into absence, because dust production drops off inversely to the third or fourth power of distance (Shannon & Wu 2011). Nevertheless, we henceforth characterize our discs in two regions, from (i) 40–150 au, and (ii) 40–1000 au.

Table 1. The number and per cent of planetesimals from an initial annulus of 40–1000 au remaining after 10, 90, and 100 Myr in our cluster simulations. The four highlighted systems in the first column are used in separate figures throughout the paper.

Highlighted systems	0 Myr	10 Myr	90 Myr	100 Myr
	2000	2000	2000	2000 (100 per cent)
	2000	2000	1996	1996 (99.8 per cent)
System #3	2000	1989	1963	1963 (98.2 per cent)
System #4	2000	1985	1958	1957 (97.9 per cent)
	2000	2000	1645	1641 (82.1 per cent)
	2000	2000	1515	1507 (75.3 per cent)
	2000	1714	961	957 (47.9 per cent)
System #1	2000	1832	853	853 (42.7 per cent)
	2000	1985	725	719 (36.0 per cent)
System #2	2000	1221	193	193 (9.7 per cent)
	2000	917	60	57 (2.9 per cent)

2.4 Results from star cluster simulations

The key results of these simulations are: (i) flybys are rarely intrusive enough to non-negligibly alter the orbital parameters of the major planets, (ii) the resulting distributions of the planetesimal discs differ substantially between systems, reflective of the perturbative environment in which they were placed, and (iii) the observed debris disc range (40–150) au is well protected from cluster perturbations except in extreme cases. For example, the fraction of surviving planetesimals after 100 Myr in the 11 systems span almost the entire possible range; see Table 1 for the 40–1000 au sample, and Table 2 for the 40–150 au sample.

Fig. 3 provides detailed illustrations for two of these systems for the entire 40–1000 au disc. The left-hand panels show the system with 43 per cent surviving planetesimals (labelled 'system #1') and the right-hand panels show the system with 9.7 per cent surviving planetesimals (labelled 'system #2'). The top, middle, and bottom panels, respectively, illustrate the semimajor axis, eccentricity, and inclination distributions. The left-hand and right-hand panels provide different viewpoints on each distribution. The fraction of surviving planetesimals for the inner 40–150 au regions of both systems is 100 per cent, and hence is not shown separately.

[3] https://www.astro.uni-jena.de/index.php/theory/catalog-of-resolved-debris-disks.html

Table 2. The number and per cent of planetesimals from an initial annulus of 40–150 au remaining after 10, 90, and 100 Myr in our cluster simulations. The system order listed is the same as in Table 1, even though here the per cent of escaped systems is not monotonically decreasing.

Highlighted systems	0 Myr	10 Myr	90 Myr	100 Myr
	225	225	225	225 (100 per cent)
	225	225	225	225 (100 per cent)
System #3	225	225	225	225 (100 per cent)
System #4	225	225	225	225 (100 per cent)
	225	225	225	225 (100 per cent)
	225	225	225	225 (100 per cent)
	225	225	200	200 (88.9 per cent)
System #1	225	225	225	225 (100 per cent)
	225	225	225	225 (100 per cent)
System #2	225	225	153	153 (68.0 per cent)
	225	225	26	26 (11.6 per cent)

The figure reveals that the outermost regions of each planetesimal disc are stripped. Other systems (not shown) that retain nearly their entire planetesimal discs harbour a more homogeneous distribution of semimajor axes throughout the 100 Myr cluster evolution. Fig. 3 also illustrates how initially circular and coplanar planetesimal orbit distributions fan out in eccentricity and inclination space. The four snapshots in time which are displayed in the figures demonstrate the significant extent of the dynamical excitation from 0 to 10 Myr and the insignificant evolution from 90 to 100 Myr; i.e. by 100 Myr, the systems have effectively dynamically settled (see also van Elteren et al. 2019).

3 MAIN-SEQUENCE EVOLUTION

At $t = 100$ Myr, we assume that the planetary systems have left the cluster environment and evolve for the remainder of the star's main-sequence evolution 'in the field'. The duration of the main-sequence evolution (about 11 Gyr) is determined by assuming that the star's initial mass and metallicity are the same as the Sun's. Variations in this value will arise depending on the stellar model used, but do not noticeably affect the final qualitative result.

Unlike in the previous section, numerically integrating the planetary systems for the entire 11 Gyr is not computationally feasible. The primary factors that restrict the time-scale for such integrations are the total number of bodies and the presence of the exo-Jupiter (the planet with the shortest orbital period, unless a planetesimal is perturbed within 5 au of the star at some epoch). Therefore, we proceed (i) by arguing that the planetesimal evolution is negligible during this phase, and (ii) supporting this argument with limited duration integrations.

3.1 Argument for negligible evolution

We begin our argument by asserting that close stellar flybys in the field are infrequent and fast compared to those in the cluster environment. Further, the Milky Way Galaxy is a collisionless system. Because the relaxation time in the Solar neighbourhood is longer than a Hubble time (see Binney & Tremaine 2008), major encounters are rare after the cluster dissolves (Portegies Zwart & Jílková 2015). Consequently, over an 11 Gyr time-scale, the expected single closest encounter distance with a planetary system is on the order of several hundred au (Zakamska & Tremaine 2004; Veras & Moeckel 2012; Correa-Otto & Gil-Hutton 2017). Hence, for this particular closest encounter, whether an individual planetesimal at that distance would be significantly perturbed becomes a function of geometry.

Additionally, because the main-sequence lifetime of 11 Gyr is two orders of magnitude higher than the 100 Myr cluster time-scale, additional processes that act over long time-scales need to be considered at this stage. Three of these processes are Galactic tides, collisional grinding, and radiative forces.

3.1.1 Galactic tides

The consequences of Galactic tides are a strong function of stellar density (or location in the Milky Way), inclination with respect to the Galactic disc, and planetesimal–star separation. If, for example, our simulated systems were in the Galactic bulge, then Galactic tides acting over 10 Gyr would significantly affect planetesimal discs (Veras & Evans 2013a). However, in the Solar neighbourhood, the effect is muted: the orbital eccentricity of a highly inclined Sedna-like object (with a semimajor axis of about 550 au and eccentricity of about 0.85) may change by a maximum of about 0.05 due to tides (Veras & Evans 2013b). Because all of our planetesimals have semimajor axes within a factor of two of Sedna's, their eccentricity changes due to tides are likely to be comparable to those from stellar flybys (just over much longer time-scales).

We note that the Galactic environment of a planetary system likely changes with time. In fact, stars migrate in the Galaxy through interaction with time-varying spiral arms in a process called 'churning' (Sellwood & Binney 2002). Our present understanding of the Galactic metallicity gradients and age–metallicity relations suggests that the Sun was born 1–3 kpc closer to the Galactic Centre than its current location (Minchev, Chiappini & Martig 2013; Frankel et al. 2018; Minchev et al. 2018; Feltzing, Bowers & Agertz 2020). This distance is comparable to the scale length of the Galactic thin disc (Bland-Hawthorn & Gerhard 2016), and so field star densities at the Solar birth radius could have been higher than the present value by a factor of a few. We are therefore slightly underestimating the impact of field star encounters and Galactic tides in this section.

3.1.2 Collisional grinding

Collisional grinding amongst planetesimals would not eject planetesimals nor their fragments from their original annulus. Instead, the consequence of mutual collisions between planetesimals is a change in their size distribution (Dohnanyi 1969; Bottke et al. 2005). This alteration does not affect the way we represent our systems in our numerical integrations because we model our planetesimals as massless point particles, and do not make assumptions about the initial masses of our disc. Further, the physical evolution of our surviving large planetesimals (>100 km) is independent of our main results, because we know a posteriori that these objects will not pollute the eventual white dwarf, and become interstellar planetesimals at a negligible rate compared with those generated from the initial cluster evolution.

The consequence of changing the size distribution is that the ground-down planetesimals may become small enough to be affected physically and orbitally by stellar radiation (see Section 3.1.3), particularly during the giant branch phases of stellar evolution (see Section 4.1.3). Hence, if one imposes a size and mass distribution on to our massless particles, then depending on these parameters, no 100 km-sized planetesimals may survive throughout

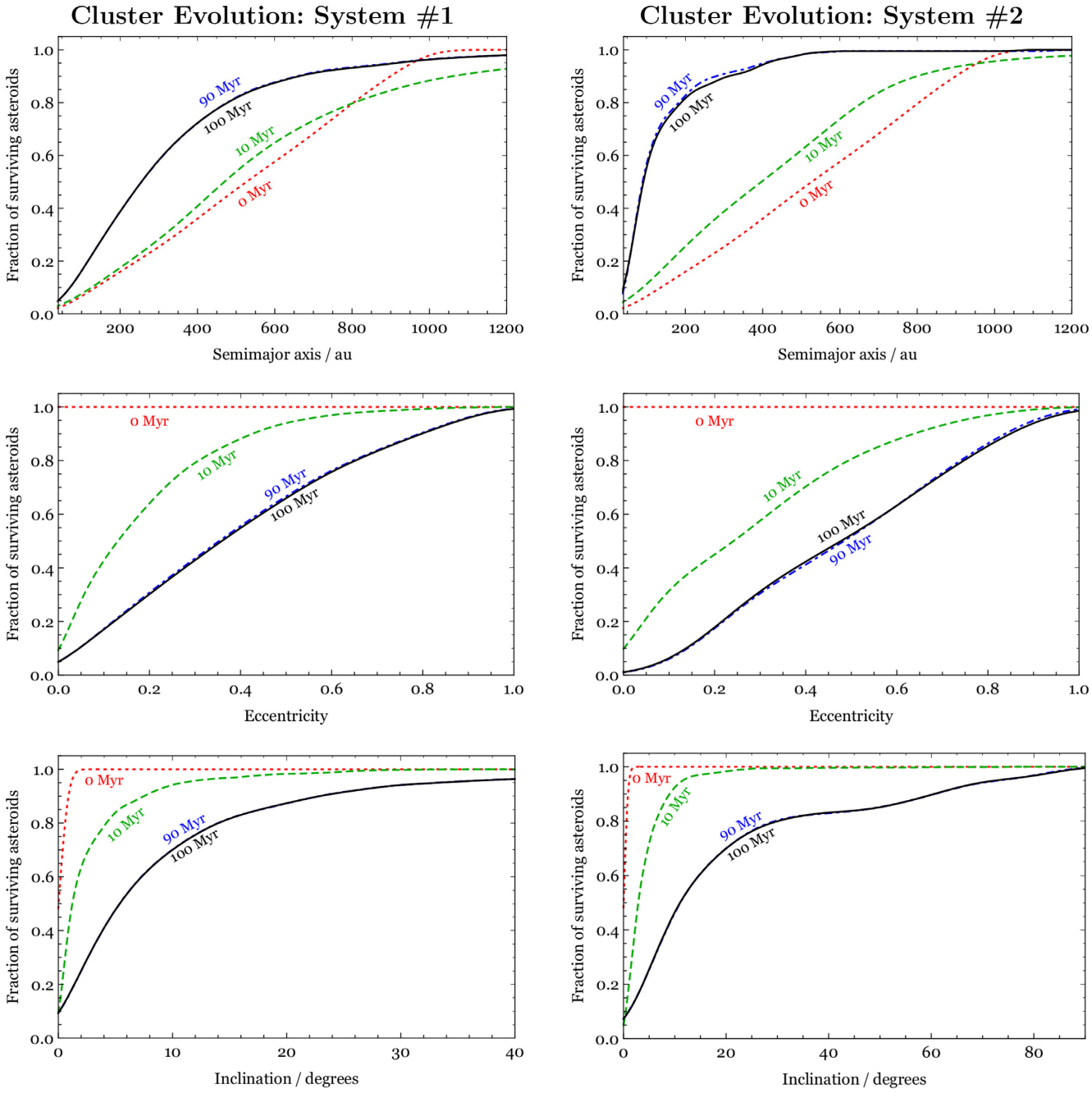

Figure 3. Cumulative distribution functions of semimajor axes (top panels), eccentricities (middle panels), and inclinations (bottom panels) for the time evolution of 2000 exo-planetesimals in initially 40–1000 au orbits subject to perturbations from a stellar birth cluster and four interior giant planets. The left-hand and right-hand panels, respectively, correspond to two different systems. In all cases, the 90 and 100 Myr curves almost entirely overlap (the 90 Myr curves are dot–dashed blue curves while the 100 Myr curves are solid black), suggesting that by 100 Myr the systems have dynamically settled.

the main sequence. The actual collisional lifetimes of objects are a non-trivial function of many parameters, including the dispersal threshold for collisions (critical specific energy), the eccentricity distribution, the inclination distribution, and the breaking radius between the gravity and strength-dominated regimes (e.g. Wyatt et al. 2007; Löhne, Krivov & Rodmann 2008). For typical parameters assumed or calculated for extrasolar debris discs, collisional evolution is not significant for objects above 100 km in size (e.g. Kenyon & Bromley 2008; Kobayashi & Löhne 2014; Krivov et al. 2018). So, in this paper, we consider only surviving planetesimals larger than 100 km (which do not change their orbital elements due to collisions).[4]

[4]For added perspective, in the Solar system, the collisional evolution of the Main belt asteroids has been investigated in a high level of detail within subsets of the belt itself (e.g. Cibulková, Brož & Benavidez 2014). The collisional evolution of the Kuiper belt is more speculative, and often based on the fraction of binary asteroids (Nesvorný et al. 2011; Dell'Oro, Cellino & Paolicchi 2012; Brunini & Zanardi 2016). Nevertheless, Kuiper belt objects greater than about 10 km in size are not thought to have undergone collisional

3.1.3 Radiative forces

Important radiative forces on planetesimals primarily arise from the YORP and Yarkovsky effects (Vokrouhlický et al. 2015). These forces describe the orbital movement (Yarkovsky effect) and the spin changes (YORP effect) from thermal imbalances created by non-zero thermal inertia and anisotropically emitted thermal radiation. The secular consequences of both effects have been observationally verified within the Main belt, despite the fantastically small accelerations produced by the Sun's radiation (often on the order of 1 pm s^{-2} for the Yarkovsky effect). The YORP effect can break apart planetesimals by spinning them up to the point of rotational fission (Holsapple 2007; Warner, Harris & Pravec 2009; Polishook et al. 2017), which primarily affects the size distribution of the fragments, rather than their orbits. Both the Yarkovsky and YORP effects are negligible at distances of at least 40 au along the main sequence, and so their contribution here can be ignored.

Overall, we argue that planetesimal disc objects with sizes $\gtrsim$100 km have orbits which vary negligibly during the 11 Gyr main-sequence phase of stellar evolution. The extent of their orbital variation should be eccentricity shifts of the order of hundredths, unless a stellar flyby achieves a particularly close encounter within hundreds of astronomical units.

3.2 Short simulations

We now attempt to support our argument by conducting feasibly short (hundreds of Myr) *N*-body simulations with a limited number of planetesimals (200 per simulation) but including both Galactic tides and stellar flybys. The results of these simulations may then be extrapolated over the entire main sequence. The planetesimals are treated as test particles and hence are not assigned masses.

We perform these simulations using the RADAU (variable time-step) integrator in the MERCURY integration package (Chambers 1999) with implemented routines for Galactic tides from Veras & Evans (2013a) and stellar flybys from Veras, Shannon & Gänsicke (2014b). We assume our systems reside in the Solar neighbourhood and adopt the corresponding numerical values associated with tides and flybys from those investigations: for the flybys, we assume a spatial stellar density of 0.392 pc^{-3} (Parravano, McKee & Hollenbach 2011) and an encounter velocity of 46 km s^{-1} (García-Sánchez et al. 2001). We also assume that the input values of the orbital elements of the planetesimals and giant planets equal the corresponding output values from our cluster simulations.[5]

Fig. 4 illustrates the time evolution of 200 randomly chosen planetesimals that survived the cluster evolution from the left-hand panels of Fig. 3. The left-hand panels of Fig. 4 include the four giant planets, and the right-hand panels do not, in order to illustrate that these planets represent the greatest driver of planetesimal orbital evolution. The middle panels display the eccentricity change from the initial values, highlighting how major planets usually vary planetesimal eccentricities by either increasing or decreasing them by orders of magnitude more than stellar flybys or Galactic tides. In the simulations in the left-hand panel, the closest stellar encounter occurred at a distance of 1786 au at 226 Myr into the simulation, whereas for the simulations in the right-hand panel, the closest stellar encounter was at 7842 au at 9.5 Myr into the simulation. Note that around these times there is no discernibly significant change in the orbital parameters.

In all cases, the eccentricity variation rarely exceeds 0.03. The two highest curves on the middle right panel correspond to the two planetesimals with semimajor axes of about 10^4 au and illustrate the secular oscillations produced from the Galactic tide; these planetesimals are outliers to the main distribution. In the simulations with major planets, only one of these 200 planetesimals becomes unstable (the jagged blue line in the upper left panel) and features the greatest eccentricity change of any planetesimal.[6]

Fig. 5 displays results for a different system (denoted 'System #3') which retained 98 per cent of its planetesimals after cluster evolution, and for which we ran the integration (200 planetesimals only) for much longer (2 Gyr) than System #1. Despite the longer time-scale, the overall result is the same as Fig. 4: planetesimal discs maintain their post-cluster orbital elements except for the outliers. The longer time-scale also allows oscillations in the orbital element distributions of these outliers (the furthest planetesimals) to be more readily detected. These oscillations arise from a combination of stellar flybys and Galactic tides. The amplitude of the inclination oscillations is highest for the most inclined (relative to the Galactic plane) planetesimal. Stellar flybys again do not appear to significantly affect the planetesimal dynamics, despite 35 close approaches within 10^4 au, with the closest approach located at 1237 au at 1.52 Gyr into the simulation.

4 GIANT BRANCH EVOLUTION

In our short main-sequence simulations, the orbital structure of the planetesimal discs remained effectively static. By assuming that later in the main sequence the disc was not significantly disturbed by a gravitational instability nor a close stellar flyby, we now consider the consequences of giant branch evolution. Giant stars undergo significant physical changes: a 1.0 $M_\odot$ star will inflate its envelope out to a distance of about 1 au, lose about half of its mass through stellar winds, and increase its luminosity by a factor of about 4×10^3.

4.1 Description of effects

4.1.1 Stellar engulfment

The expansion of the stellar envelope can directly engulf closely orbiting planets, and tidally draw into the envelope planets that reside beyond the maximum extent of the stellar envelope. This critical engulfment distance has been extensively investigated,

evolution over the last 4 Gyr or so (Brasser & Morbidelli 2013; Jutzi et al. 2017; Morbidelli & Nesvorny 2019) and hence represent remnants of early dynamical instability which involved Neptune (Wolff, Dawson & Murray-Clay 2012; Parker 2015; Chen, Ma & Zheng 2016; Nesvorný & Vokrouhlický 2016; Volk & Malhotra 2019). However, Sedna may be a remnant of collisional evolution far beyond the Kuiper belt (Silsbee & Tremaine 2018).

[5]In our stellar cluster simulations in Section 2, the cluster evolution does slightly change the orbits of the giant planets, with the exo-Neptune experiencing the largest change. The typical scale of the changes for the exo-Neptune is 0.01–0.1 au in semimajor axis, 0.005–0.025 in eccentricity, and 0.001°–1.0° in inclination.

[6]We note that if some planetesimal disc objects were initially highly eccentric, then these relatively modest eccentricity changes would be much more significant. For example, consider a body at 1000 au with a pericentre at 40 au and an eccentricity of 0.96. If its eccentricity were increased by 0.03, its pericentre would now be at just 10 au, close enough to interact with Saturn.

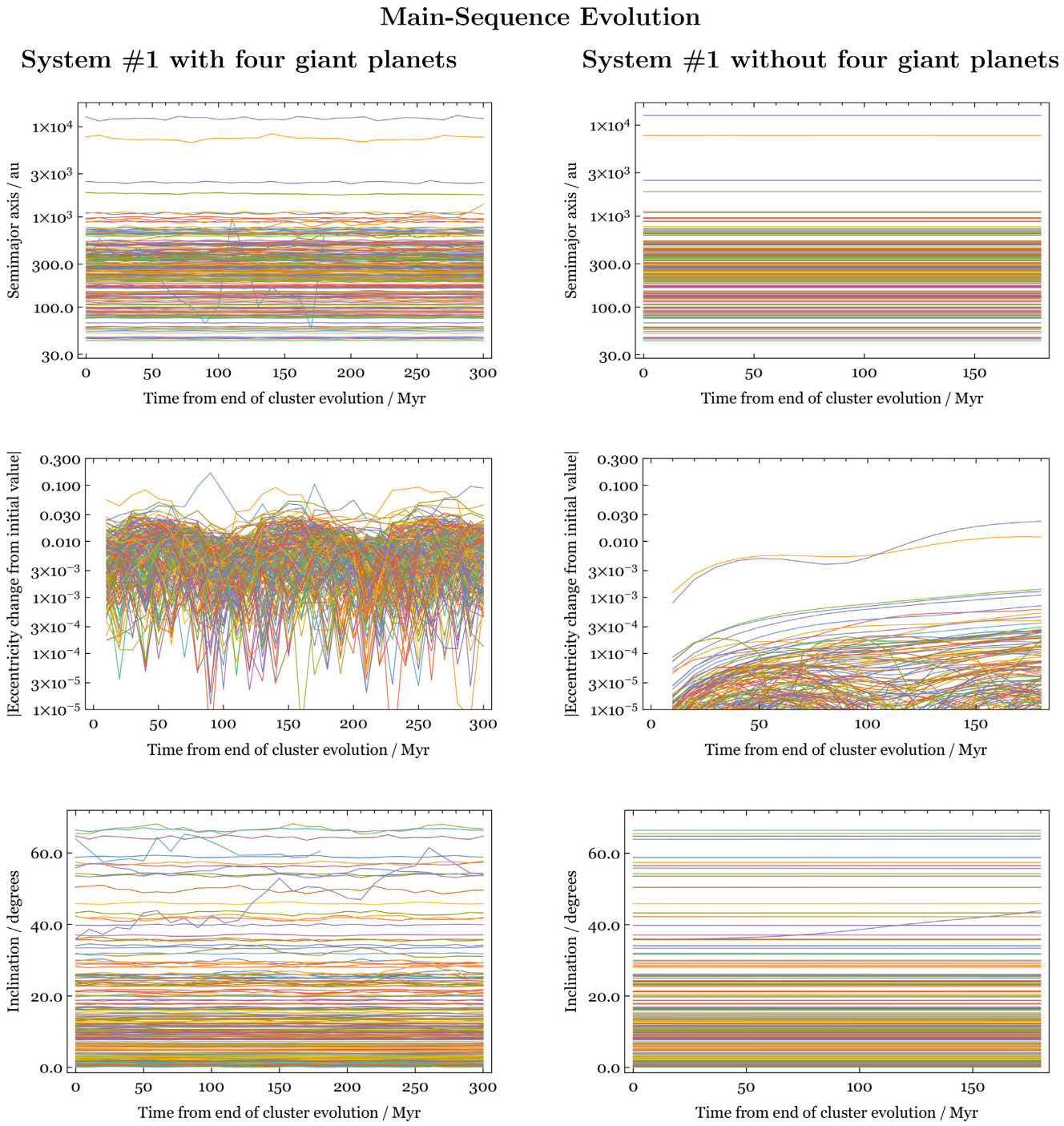

Figure 4. Main-sequence evolution (for hundreds of Myr only) of 200 planetesimals starting with their post-cluster evolution orbital parameters from Fig. 3. Included on all panels are the effects of stellar flybys and Galactic tides. The left-hand panels also include the effect of an exo-Jupiter, exo-Saturn, exo-Uranus, and exo-Neptune. The plots illustrate that the major planets are the strongest perturbers of exo-planetesimals, and that despite their presence, planetesimal discs largely maintain their structure in the absence of a violent dynamical instability.

but nevertheless varies depending on the stellar and tidal models adopted (Kunitomo et al. 2011; Mustill & Villaver 2012; Adams & Bloch 2013; Nordhaus & Spiegel 2013; Villaver et al. 2014; Madappatt, De Marco & Villaver 2016; Staff et al. 2016; Gallet et al. 2017; Rao et al. 2018; Sun et al. 2018). Regardless, all models agree that objects orbiting a 1.0 $M_{\odot}$ star beyond a few au would avoid engulfment.

Although planetesimal discs would survive engulfment, they could be affected by tides indirectly. Engulfment of planets changes the secular resonance structure of the system (Petrovich & Muñoz 2017; Smallwood et al. 2018, 2019), which may trigger instabilities (collisions or ejections) in previously stable regions. However, for Solar system analogues (Smallwood et al. 2018, 2019), where an exo-Mercury, exo-Venus, and maybe an exo-Earth would be

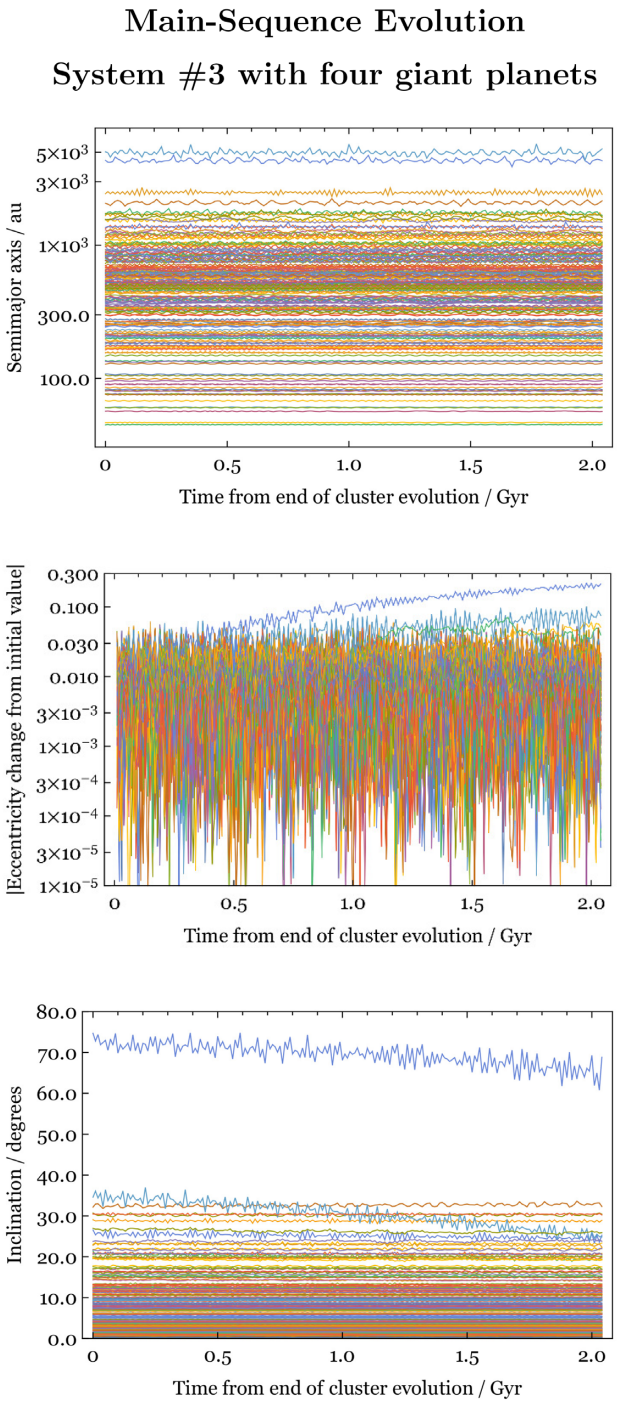

Figure 5. Like Fig. 4, but for a different system where the cluster evolution (not shown in Fig. 3) was ineffectual at removing planetesimals from an initial Kuiper belt (such that 98 per cent of the planetesimals remained stable) and for a longer simulation time-scale (2 Gyr). The resulting trends are similar to those in Fig. 4. The two planetesimals with the greatest separations and initial inclinations showcase discernible secular trends in their eccentricity and inclination temporal evolution profiles due to Galactic tides.

engulfed (Schröder & Smith 2008), the secular resonance region of greatest importance would be internal to the giant planets. Hence, we need not consider engulfment for our planetesimal discs.

4.1.2 Stellar mass-loss

Stellar mass-loss, however, must be considered. The changing potential expands the orbits of all planets and planetesimals (Omarov 1962; Hadjidemetriou 1963). If the mass-loss is assumed to be isotropic (Veras, Hadjidemetriou & Tout 2013a), then objects within about 10^3 au (including the planetesimal discs and four giant planets) would all double their semimajor axis. The extent to which their eccentricities change is positively correlated with semimajor axis, and usually neglected below a certain 'adiabatic' limit (Veras et al. 2011). For distances of 10^3 au, we should expect eccentricity shifts just of the order of hundredths. Hence, the result of stellar mass-loss on our planetesimal discs would be a larger, but self-similar, annulus.

However, although the mutual semimajor axis ratios between planetesimals and planets would not change due to adiabatic mass-loss, the decrease in mass from the central star may nevertheless trigger instability (Debes & Sigurdsson 2002). Whether and when this trigger is activated depends on number of bodies, mass of bodies, and mutual separation between the bodies (Bonsor et al. 2011; Debes et al. 2012; Mustill et al. 2013; Portegies Zwart 2013; Veras et al. 2013b; Frewen & Hansen 2014; Mustill, Veras & Villaver 2014; Veras & Gänsicke 2015; Veras et al. 2016b, 2017b, 2018). We will explore the extent of the potential instability in our planetesimal discs due to the presence of an exo-Neptune through numerical simulations.

4.1.3 Stellar luminosity

First, we comment on the effects of the increased luminosity of the host star during the giant branch phases. While grain-sized particles may be 'blown-out' by radiation pressure (Bonsor & Wyatt 2010; Dong et al. 2010; Martin et al. 2020; Zotos & Veras 2020), larger minor planets are subject to other effects. For example, the enhanced YORP effect would effectively destroy Solar system Main belt asteroids between 100 m and 10 km in size due to rotational spin-up (Veras et al. 2014a). Because the planetesimal's change in spin rate is inversely proportional to the square of both the separation and planetesimal radius, the YORP effect on 100 km planetesimals would be at least four orders of magnitude smaller. Hence, we can safely neglect the YORP effect in post-main-sequence planetesimal discs with planetesimals larger than about 100 km.

However, planetesimals that survive YORP-induced spin-up may be orbitally perturbed by the enhanced Yarkovsky effect. We can estimate the extent of the Yarkovsky effect during the giant branch phase for a 1.0 $M_\odot$ main-sequence star by using equations 108 and 110 of Veras et al. (2015b). Across the tip of the asymptotic giant branch, where the stellar luminosity is greatest, a planetesimal with a radius of 100 km and a distance of 40 au would shift[7] its semimajor axis by about 10^{-3} au and its eccentricity by about 10^{-5}. A shift of 10^{-3} au is negligible because that value is orders of magnitude smaller than the typical libration widths of strong resonances in the trans-Neptunian region. Veras et al. (2019) provide further evidence that the Yarkovsky effect for 100 km planetesimals in this region is negligible by considering a variety of limiting Yarkovsky models that place bounds on the motion.

[7]These estimates are about the same orders of magnitude as the excitations expected from the integrated monotonic Yarkovsky drift across the 11 Gyr main-sequence evolution.

4.1.4 Galactic tides and stellar flybys

Regarding Galactic tides and stellar flybys during the giant branch phases, the primary difference from the main-sequence phase is the time-scale over which these perturbations act. The durations of the main-sequence, red giant branch, and asymptotic giant branch phases for a Sun-like star are about 11 Gyr, 1.5 Gyr, and 5 Myr, respectively. These differences indicate that Galactic tides and stellar flybys are less disruptive during the giant branch phases than on the main sequence. Fig. 3 of Veras et al. (2014c) plots the relative importance of Galactic tides, stellar flybys, and stellar mass-loss for the planets orbiting red giant branch and asymptotic giant branch stars as a function of stellar mass and Galactocentric distance. That figure illustrates that we can neglect Galactic tides and stellar flybys during the giant branch phases of stellar evolution.

4.1.5 Collisional grinding

Collisional evolution within the disc during giant branch evolution follows the description in Section 3.1.2, except now the stellar mass is a function of time. Bonsor & Wyatt (2010) analysed this case, and found that the collisional lifetime increases as the star loses mass. The primary reason is because this stellar mass-loss expands the disc and increases the pairwise distance amongst all of its contents. The planetesimals are hence 'safer' during giant branch evolution than along the main sequence.

4.2 Numerical simulations

We now perform *N*-body numerical simulations to quantify the changes in the orbital architectures of planetesimal discs during the giant branch phases of evolution. The above discussion suggests that we can neglect radiative forces (assuming our test particles are larger than about 100 km), any residual effects from the engulfment of terrestrial planets, and external perturbers. What remains to be explored by these simulations is potential instability triggered by mass-loss with Neptune and the planetesimals (we know that the giant planets themselves will remain stable from Veras 2016b).

The code we adopt in this section is different from the individual codes used in Sections 2 and 3 (see Fig. 1). Here, because we must concurrently model stellar and planetary evolution, we use the code presented in Mustill et al. (2018). This code is an updated version from the one that was first presented in Veras et al. (2013b) and uses the RADAU integrator from the MERCURY integration package (Chambers 1999).

We choose RADAU as the integrator because it is non-symplectic (allowing it to handle an arbitrarily changing potential) but very accurate, being able to accurately track not only a planet's semimajor axis but also its orbital phase. We adopt a tolerance value for the RADAU integrator of 10^{-11}. The stellar evolution input is provided by the SSE code (Hurley et al. 2000). The output from the stellar evolution code is fed to MERCURY, where the stellar mass is updated at every subdivision of a time-step for the force calculations. The stellar radius is updated every time-step, when checks are made for the removal of particles by collision with the star (no collisions occurred in our simulations).

We adopt the default numerical parameters in the SSE code for our simulations. Among these is the Reimers mass-loss coefficient, which is set to 0.5. This coefficient dictates the time evolution of the mass-loss. Veras & Wyatt (2012) sampled a realistic range of these coefficients for the future evolution of the Sun, and found that the total amount of mass lost ranges from about 0.465 to 0.490 $M_\odot$ depending on the choice of coefficient. Also, the time at which the asymptotic giant branch phase is initiated can vary by hundreds of Myr depending on this coefficient choice. Further, higher coefficients produce greater mass-loss rates, yielding a Solar system post-main-sequence escape boundary range of 10^3–10^4 au (well beyond the outer boundary of most of our planetesimals). These variations due to coefficient choice are not sufficiently large to warrant partitioning the available computational resources in order to sample different coefficients.

As justified in Section 3, we adopt for our initial conditions the outputted values of the simulations performed in Section 2. We begin our simulations right before the start of the red giant branch phase, which is 10.94 Gyr after the instance of zero-age main sequence (ZAMS). We run these simulations for the entire duration of the giant branch phases (1.5 Gyr) plus during the start of the white dwarf phase, for 8 Gyr in System #1 and 2.4 Gyr in another system denoted System #4.

Fig. 6 illustrates the results for System #1. The doubling of the semimajor axes occurs in two distinct steps, corresponding to the tips of the red giant and asymptotic giant branch phases around 1.5 Gyr into the simulation. During this time, a planetesimal's eccentricity variation is shifted upwards by an amount which is correlated to semimajor axis: roughly, for 10^2, 10^3, and 10^4 au, eccentricity variation is changed respectively to 10^{-3}, 10^{-2}, and 10^{-1}. The inclination remains unaltered by mass-loss, an expected result when the mass-loss is isotropic (Veras et al. 2013a; Dosopoulou & Kalogera 2016a, b). Further, the mutual inclination between the major planets and the planetesimals during the mass-loss episode is not expected to contribute to possible instability (Veras et al. 2018).

The plots in Fig. 6 do illustrate some instability, which is to be expected. However, only 5 of the 200 planetesimals simulated become unstable, meaning that the planetesimal disc remains relatively undisturbed, just with double the semimajor axis and a usually negligible eccentricity shift.

The occurrence of instability is stochastic. In order to test how the extent of instability changes due to chaos, in Fig. 7 we show the evolution of a different system (denoted system #4) of 70 planetesimals, where the integration was repeated three times with the same initial conditions. However, in each case the integration was interrupted and restarted at different times during the giant branch evolution. Each plot exhibits different variations in the oscillations of each curve, and in three of the four plots, one planetesimal becomes unstable (in the other there is no instability). The robustness of the evolution in all cases suggests that the variations in instabilities introduced by stochasticity do not affect our conclusions.

5 WHITE DWARF EVOLUTION

Evolution during the white dwarf phase proceeds similarly to that along the main-sequence phase (Section 3), but with a few differences. The largest objects ($\gtrsim$100 km) in the planetesimal disc now occupy a (primarily) 80–2000 au annulus, from originally a 40–1000 au annulus. Further, the time-scale for white dwarf cooling can reach a Hubble time (>13 Gyr), although the oldest known metal-polluted white dwarf has a cooling age of about 8 Gyr (Hollands et al. 2017; Hollands, Gänsicke & Koester 2018).[8]

[8] A white dwarf with a cooling age of 8 Gyr corresponds to a main-sequence progenitor mass larger than the 1.0 $M_\odot$ that we considered here. Older

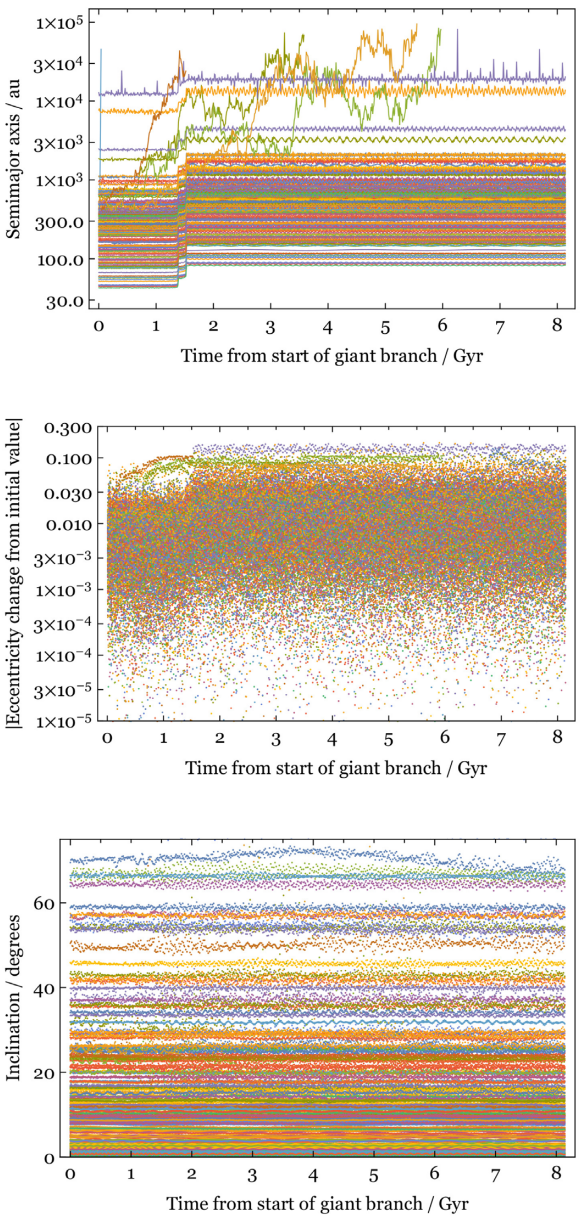

Figure 6. Post-main-sequence evolution for the same system in the left-hand panels of Fig. 3 and in Fig. 4. The evolutions in the bottom two panels are illustrated with points rather than joined lines for greater clarity. Despite a few instabilities, 97.5 per cent of the post-cluster planetesimal disc remains intact, with an eccentricity variation of typically no more than a few hundredths, and an expected doubling of its semimajor axis.

White dwarf luminosities monotonically decrease from the moment they are born (e.g. Mestel 1952). This fact, coupled with the extended semimajor axes of the planetesimals, illustrates that the Yarkovsky and YORP effects are negligible for the $\gtrsim$100 km objects. We note importantly, however, that boulders and pebbles may still be significantly affected by this radiation around young white dwarfs (Veras 2020), where even the weaker force generated by Poynting–Robertson drag may crowd the region around the white dwarf with debris (Stone et al. 2015; Veras et al. 2015c).

We can estimate the consequences of doubling of the semimajor axis of our planetesimal discs with respect to external forces. For Galactic tides, Veras & Evans (2013b) defined two different regimes: 'adiabatic' and 'non-adiabatic' (similar to the terms used for mass-loss), where the adiabatic regime is defined by when the orbital time-scale is faster than the Galactic tidal time-scale. They showed how the equations of motion differ in these two regimes. The planetesimal discs here are comfortably within the adiabatic regime (Veras et al. 2014c), where Galactic tides do not alter the semimajor axis a, but vary the eccentricity and inclination by an amount proportional to $a^{3/2}$. Further, for stellar flybys, equation 46 of Veras & Moeckel (2012) indicates that the number of flybys which trigger an orbital eccentricity exceeding a given value is, roughly, also proportional to $a^{3/2}$. Hence, doubling the semimajor axis increases the eccentricity excitation from external forces approximately by a factor of 2.8. Consequently, for this eccentricity variation to reach 0.1 during the white dwarf phase, it would need to be at the 0.03 level during the main sequence.

Such eccentricity variations are important only if they are already on a highly eccentric orbit or could trigger instability with a sufficiently close major planet. Instability with the exo-Neptune is the primary driver of orbital architecture variation of an exo-Kuiper belt during the white dwarf phase. Bonsor et al. (2011) quantified how a single planet orbiting a white dwarf could drive external exo-Kuiper belt objects out of their annulus inward, and Mustill et al. (2018) did the same, but for systems of three major planets. Mustill et al. (2018) demonstrated that in order for these objects to actually reach the Roche radius of the white dwarf (and hence pollute it), a gravitational instability amongst multiple major planets is necessary. Instability amongst terrestrial planets provides a much better match to the observed pollution rate as a function of time (Hollands et al. 2018) than do giant planets (such as the Solar system giant planets).

Because Jupiter, Saturn, Uranus, and Neptune are expected to remain stable through at least 10 Gyr of Solar white dwarf cooling (Laskar & Gastineau 2009; Hayes et al. 2010; Zeebe 2015; Veras 2016b), we hence do not expect scattered disc objects such as Sedna to pollute the Solar white dwarf. The orbital elements of these scattered disc objects will have not significantly changed since the last scattering event (either amongst planets or from stellar flybys). In Solar system analogues with no such scattering events, the orbital elements should reflect the values attained at the end of stellar cluster dispersion.

6 DISCUSSION

Our study aimed to achieve a qualitative understanding of how the largest ($\gtrsim$100 km) planetesimal disc objects evolve through time. We focused on the initial semimajor axis range 40–1000 au. Planetesimals likely formed in a more restricted range; as discussed earlier, observations of debris discs indicate that their maximal radial extent is approximately 150 au. Nevertheless, because we adopted test particles, we were able to explore locations exterior to 150 au to which a planetesimal might have been perturbed.

Our results do not profess to answer, but instead provide a foundation for, tackling major topical questions, such as: what is the frequency of interstellar interlopers within the Solar system from

polluted systems may exist but are difficult to detect because of their faintness.

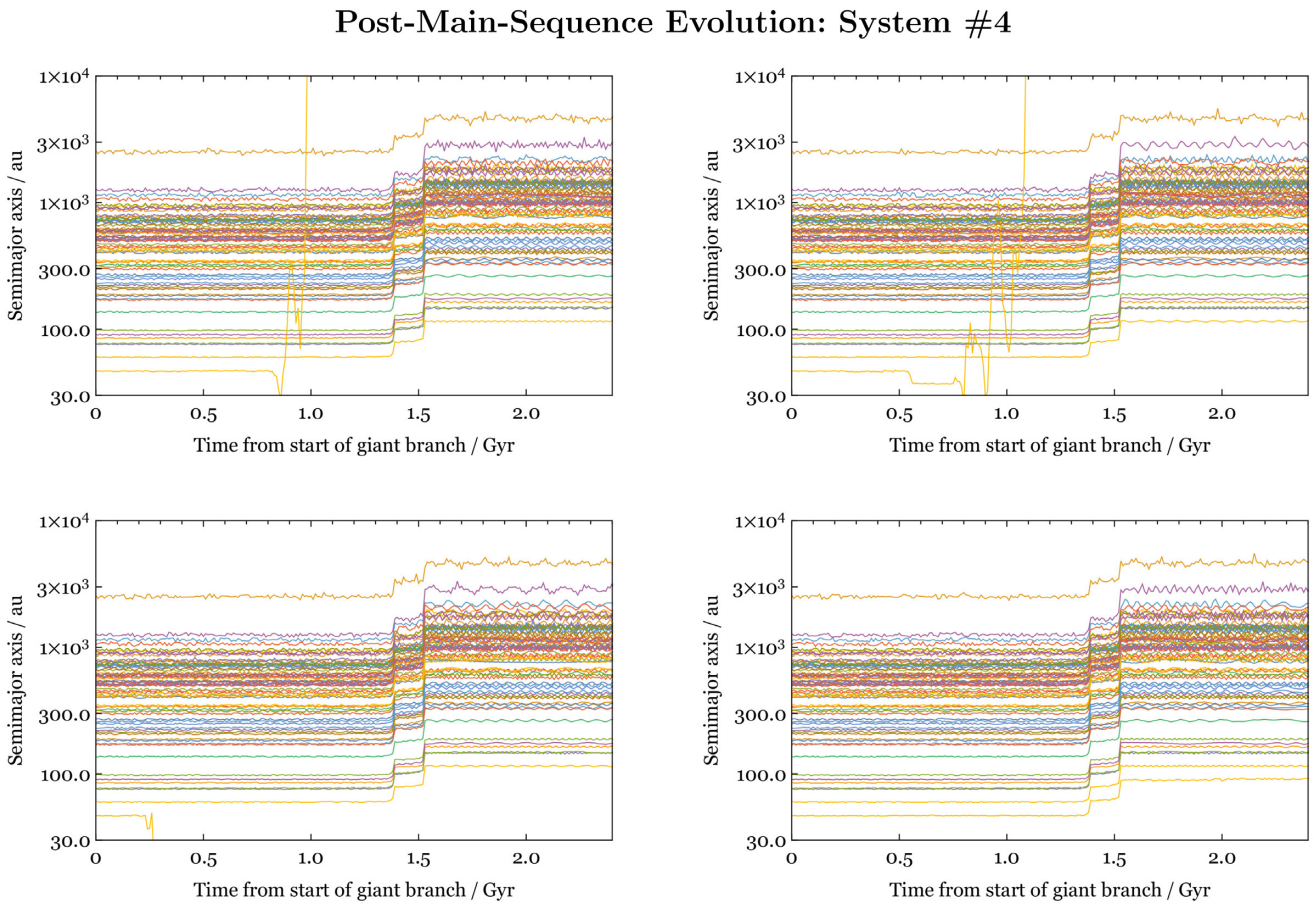

Figure 7. Repeat post-main-sequence simulations of the same 70 planetesimals in order to indicate how the chaotic nature of these systems alters their unstable fraction. In three of the four systems, one planetesimal becomes unstable, whereas in the other, all planetesimals remain stable.

post-main-sequence ejection (Do et al. 2018; Rafikov 2018; Moro-Martín 2019)? (Section 6.1), and what is the dominant delivery mechanism in metal-polluted white dwarf systems (Veras 2016a)? (Section 6.2)

Obtaining answers to both questions requires a comparative population analysis, which we now perform.

6.1 Implications for white dwarf pollution

The mass reservoirs that primarily generate white dwarf pollution are still unknown. One candidate reservoir is the population of large exo-Kuiper belt planetesimals, which has been the focus of this study.

This reservoir is particularly important to consider because Bonsor et al. (2011) demonstrated that a Neptune analogue at a 30 au separation from the star could scatter a sufficient amount of exo-Kuiper belt material extending out from 30 to about 48 au towards the white dwarf to explain metal accretion rates. This conclusion is strongly dependent on the belt structure and the time at which the belt was initialized. Unlike our study, Bonsor et al. (2011) modelled planetesimals that were much closer to the planet and hence much more conducive to instabilities due to overlapping resonances. They also performed integrations along main-sequence evolution for just 10^7 yr (to dynamically settle the belt), followed by integrations during giant branch evolution.

Hence, placing that study into context is important when comparing the amount of pollution that has been generated in both studies. Bonsor et al. (2011) did not perform stellar cluster simulations and we did not consider planetesimals closer to (within 40 au) the exo-Neptune. Further, we note that our nil result for pollution should not imply that planetesimals at or slightly beyond 40 au can never pollute white dwarfs. Major planets could exist beyond 30 au (a notable example being the HR 8799 system; Marois et al. 2008, 2010) and could generate the same type of instability that was showcased in Bonsor et al. (2011) in those regions to generate pollution.

Further, by considering an annulus of planetesimals extending out to 10^3 au, we also have probed pollution prospects towards the inner exo-Oort-cloud. Separations out to 10^3 au have previously been largely unexplored, as previous exo-Oort cloud-based studies have modelled minor planets in the separation range 10^3–10^4 au (Caiazzo & Heyl 2017), 1×10^3–5×10^4 au (Stone et al. 2015), and 10^4–10^5 au (Veras et al. 2014b).

The numerical integrations in all these studies of planetesimals beyond 10^3 au yielded non-zero quantities of white dwarf pollutants, partially triggered by excitation due to giant branch mass-loss (Veras & Wyatt 2012; Veras et al. 2014b, c). These excited planetesimals evolve non-adiabatically in both the mass-loss (Veras et al. 2011) and Galactic tidal (Veras et al. 2014c) senses (meaning that their orbital evolution due to each force cannot be characterized in a closed explicit form), and hence are actually more likely to strike

the white dwarf than planetesimals in our initial separation range of 40–1000 au.[9]

We conclude that the range 40–10^3 au represents a 'sweet spot' where we would not expect pollutants dynamically, at least for Solar system analogues. Further, chemically, most pollutants are rocky (Zuckerman et al. 2007; Gänsicke et al. 2012; Jura & Young 2014; Harrison, Bonsor & Madhusudhan 2018; Hollands et al. 2018; Doyle et al. 2019; Swan et al. 2019b; Xu et al. 2019; Bonsor et al. 2020) rather than volatile rich (Xu et al. 2017), suggesting that the main source of pollutants lies inward of 30 au. Despite this chemical suggestion, which has increased in robustness over the last few years, many investigations have dynamically invoked the reservoir of planetesimals initially beyond 30 au as a viable source of white dwarf pollution (Bonsor et al. 2011; Veras et al. 2014b; Stone et al. 2015; Caiazzo & Heyl 2017; Veras & Kurosawa 2020), helping to motivate our study.

6.2 Implications for interstellar planetesimals

Another motivation for our investigation is to explore the effect of 'full-lifetime evolution' on the eventual ejection of planetesimals from an initial 40–1000 au disc. The flux of such planetesimals in space is unknown, but was predicted to be large enough to produce interstellar interlopers, even before the discovery of 1I/'Oumuamua (Moro-Martín, Turner & Loeb 2009). These planetesimals provide important probes of the outer parts of planetary systems, probes that are not yet available by other means (McGlynn & Chapman 1989; Stern 1990; Wyatt et al. 2017).

After the discovery of 1I/'Oumuamua, theoretical investigations of interstellar interlopers blossomed (e.g. Do et al. 2018; Jackson et al. 2018; Katz 2018; Moro-Martín 2018, 2019; Portegies Zwart et al. 2018; Rafikov 2018; Raymond et al. 2018a; Raymond, Armitage & Veras 2018b; 'Oumuamua ISSI Team 2019; Malamud & Perets 2020), ensuring that our study is timely. Because those other studies focus on individual aspects of generating and delivering these planetesimals to the Solar system, a comprehensive framework is needed to consolidate the plethora of ideas posed.

We do not claim to provide such a framework. However, what we do, for the first time, is bring together all phases of stellar evolution in a self-consistent way for the 40–1000 au region. Our findings are similar to our result for white dwarf pollution: dynamical stagnation. Just as our planetesimals do not collide with the star, they also rarely escape after the stellar cluster phase.

During the cluster phase, we showed that for the 40–1000 au semimajor axis region, the escape fraction could be any value depending on the physical and orbital properties of the stars in the cluster (in Table 1, the escape fraction during the cluster phase ranged from 2.9 per cent to 100 per cent). This result was not a priori trivial because the planetesimals were initially dynamically cold (on circular and coplanar orbits), and with a maximum semimajor axis that was set at just 1000 au, which is two orders of magnitude smaller than the typical Hill ellipsoid axes of a planetary system (Veras et al. 2014c).

[9]We note that none of these studies have explicitly explored the sensitive dependence of exo-Oort-cloud evolution on the specific Galactic model adopted (Portegies Zwart et al. 2018; Torres et al. 2019) nor exchange mechanisms with both planetesimal discs (Weissman & Levison 1997; Shannon et al. 2015; Shannon, Jackson & Wyatt 2019) and the interstellar medium (Heisler & Tremaine 1986).

In subsequent phases of stellar evolution, the ejection fraction is comparatively negligible. As we illustrated in Figs 4–5, ejection does not occur along the main sequence except during a chance, particularly close flyby. During post-main-sequence evolution, ejection is more likely, but only at the few per cent level (see Fig. 6), and sometimes not at all (Fig. 7).

Consequently, we conclude that for the 40–1000 au range, ejection predominantly occurs during the early cluster phase. Although post-main-sequence origins of interlopers like 1I/'Oumuamua and 2I/Borisov are possible, in this context tidal disruption events around white dwarfs (Rafikov 2018; Malamud & Perets 2020) may be more likely to occur than ejection during the giant branch phases.

Despite how our conclusion about ejection occurring primarily during the cluster phase is solely based on 1.0 $M_\odot$ stars with four giant planets, we speculate that this conclusion is robust throughout the Galaxy: although the highest mass white dwarf progenitors would yield the greatest giant branch excitation and ejection potential (Veras et al. 2011, 2020b), most stars in the Milky Way are actually less massive than the Sun.

7 CONCLUSION

Both metal-polluted white dwarfs and the interstellar planetesimals 1I/'Oumuamua and 2I/Borisov provide strong motivation for investigating the full life cycle of minor planets. Here, we take one step towards achieving this understanding by focusing on large ($\gtrsim$100 km) planetesimals in an initial semimajor axis range of 40–1000 au, which corresponds to a planetesimal disc or exo-Kuiper belt.

For the first time, we attempted to link the formative pathways of these belts from their stellar birth cluster to their fate, when the star leaves the main sequence and eventually transforms into a white dwarf. We performed this task through a series of arguments and simulations which encompass the strongest forces on these planetesimals, from stellar radiation to mutual, external, and major planet perturbations in Solar system analogues. We found that the planetesimal orbital distributions obtained at the end of stellar cluster evolution can be used to predict the evolved form of these distributions during the white dwarf phase unless a major gravitational instability (amongst major planets or with a passing star) occurred in-between. This prediction just entails inflating the planetesimal semimajor axes by an amount that is inversely proportional to the stellar mass-loss; the 40–1000 au range represents a 'sweet spot' where other forces are ineffectual at producing major changes.

ACKNOWLEDGEMENTS

We thank the referee for their insightful and detailed comments, which have significantly improved the manuscript. DV gratefully acknowledges the support of the STFC via an Ernest Rutherford Fellowship (grant ST/P003850/1). KR and RS acknowledge the support of the DFG priority program SPP 1992 'Exploring the Diversity of Extrasolar Planets' (SP 345/20–1). FFD and MBNK were supported by the Research Development Fund (grant RDF-16-01-16) of Xi'an Jiaotong-Liverpool University (XJTLU), and MBNK acknowledges support from the National Natural Science Foundation of China (grant 11573004). MXC thanks Santiago Torres and Diptajyoti Mukherjee for insightful discussions. AJM acknowledges funding from the Knut and Alice Wallenberg Foundation (project grant 2014.0017) and the Swedish Research Council (starting grant 2017-04945). AS is supported by funding from the European Research Council under the European Community's H2020 (2014-2020/ERC

Grant Agreement No. 669416 'LUCKY STAR'). RS has been supported by National Astronomical Observatories of Chinese Academy of Sciences, Silk Road Project, and by National Natural Science Foundation of China under grant No. 11673032. Star cluster simulations have been done on the GPU accelerated cluster 'kepler', funded by Volkswagen Foundation grants 84678/84680.

REFERENCES

Aarseth S. J., 1999, Celest. Mech. Dyn. Astron., 73, 127
Adams F. C., 2010, ARA&A, 48, 47
Adams F. C., Bloch A. M., 2013, ApJ, 777, L30
Adams F. C., Hollenbach D., Laughlin G., Gorti U., 2004, ApJ, 611, 360
Alcock C., Fristrom C. C., Siegelman R., 1986, ApJ, 302, 462
Anderson K. R., Adams F. C., Calvet N., 2013, ApJ, 774, 9
Andrews S. M., 2020, ARA&A , preprint(arXiv:2001.05007)
Antoniadou K. I., Veras D., 2016, MNRAS, 463, 4108
Antoniadou K. I., Veras D., 2019, A&A, 629, A126
Batygin K., Adams F. C., Batygin Y. K., Petigura E. A., 2020, AJ, 159, 101
Belczynski K., Kalogera V., Bulik T., 2002, ApJ, 572, 407
Binney J., Tremaine S., 2008, Galactic Dynamics, 2nd edn. Princeton University Press, Princeton, NJ
Bland-Hawthorn J., Gerhard O., 2016, ARA&A, 54, 529
Bonsor A., Veras D., 2015, MNRAS, 454, 53
Bonsor A., Wyatt M., 2010, MNRAS, 409, 1631
Bonsor A., Mustill A. J., Wyatt M. C., 2011, MNRAS, 414, 930
Bonsor A., Kennedy G. M., Crepp J. R., Johnson J. A., Wyatt M. C., Sibthorpe B., Su K. Y. L., 2013, MNRAS, 431, 3025
Bonsor A., Kennedy G. M., Wyatt M. C., Johnson J. A., Sibthorpe B., 2014, MNRAS, 437, 3288
Bonsor A., Carter P. J., Hollands M., Gänsicke B. T., Leinhardt Z., Harrison J. H. D., 2020, MNRAS, 492, 2683
Bottke W. F., Durda D. D., Nesvorný D., Jedicke R., Morbidelli A., Vokrouhlický D., Levison H. F., 2005, Icarus, 179, 63
Brasser R., Morbidelli A., 2013, Icarus, 225, 40
Brasser R., Duncan M. J., Levison H. F., 2006, Icarus, 184, 59
Brown J. C., Veras D., Gänsicke B. T., 2017, MNRAS, 468, 1575
Brucalassi A. et al., 2017, A&A, 603, A85
Brunini A., Zanardi M., 2016, MNRAS, 455, 4487
Cai M. X., Meiron Y., Kouwenhoven M. B. N., Assmann P., Spurzem R., 2015, ApJS, 219, 31
Cai M. X., Gieles M., Heggie D. C., Varri A. L., 2016, MNRAS, 455, 596
Cai M. X., Kouwenhoven M. B. N., Portegies Zwart S. F., Spurzem R., 2017, MNRAS, 470, 4337
Cai M. X., Portegies Zwart S., van Elteren A., 2018, MNRAS, 474, 5114
Cai M. X., Portegies Zwart S., Kouwenhoven M. B. N., Spurzem R., 2019, MNRAS, 489, 4311
Caiazzo I., Heyl J. S., 2017, MNRAS, 469, 2750
Carrera D., Gorti U., Johansen A., Davies M. B., 2017, ApJ, 839, 16
Chambers J. E., 1999, MNRAS, 304, 793
Chen Y.-Y., Ma Y., Zheng J., 2016, MNRAS, 458, 4277
Cibulková H., Brož M., Benavidez P. G., 2014, Icarus, 241, 358
Concha-Ramírez F., Wilhelm M. J. C., Portegies Zwart S., Haworth T. J., 2019, MNRAS, 490, 5678
Correa-Otto J. A., Gil-Hutton R. A., 2017, A&A, 608, A116
Coutu S., Dufour P., Bergeron P., Blouin S., Loranger E., Allard N. F., Dunlap B. H., 2019, ApJ, 885, 74
Dai Y.-Z., Liu H.-G., Wu W.-B., Xie J.-W., Yang M., Zhang H., Zhou J.-L., 2018, MNRAS, 480, 4080
Debes J. H., Sigurdsson S., 2002, ApJ, 572, 556
Debes J. H., Walsh K. J., Stark C., 2012, ApJ, 747, 148
Dell'Oro A., Cellino A., Paolicchi P., 2012, MNRAS, 425, 1492
Dennihy E., Clemens J. C., Dunlap B. H., Fanale S. M., Fuchs J. T., Hermes J. J., 2018, ApJ, 854, 40
Do A., Tucker M. A., Tonry J., 2018, ApJ, 855, L10
Dohnanyi J. S., 1969, J. Geophys. Res., 74, 2531
Dong R., Wang Y., Lin D. N. C., Liu X.-W., 2010, ApJ, 715, 1036
Dosopoulou F., Kalogera V., 2016a, ApJ, 825, 70
Dosopoulou F., Kalogera V., 2016b, ApJ, 825, 71
Doyle A. E., Young E. D., Klein B., Zuckerman B., Schlichting H. E., 2019, Science, 366, 356
Duvvuri G., Redfield S., Veras D., 2019, submitted
Ernst A., Just A., Spurzem R., 2009, MNRAS, 399, 141
Farihi J., 2016, New Astron. Rev., 71, 9
Feltzing S., Bowers J. B., Agertz O., 2020, MNRAS, 493, 1419
Ferlet R., Hobbs L. M., Madjar A. V., 1987, A&A, 185, 267
Flammini Dotti F., Kouwenhoven M. B. N., Cai M. X., Spurzem R., 2019, MNRAS, 489, 2280
Flammini Dotti F., Cai M. X., Spurzem R., Kouwenhoven M. B. N., 2020, in Elmegreen B. G., Tóth L. V., Güdel M., eds, Proc. IAU Symp. 345, Origins: From the Protosun to the First Steps of Life. Kluwer, Dordrecht, p. 293
Frankel N., Rix H.-W., Ting Y.-S., Ness M., Hogg D. W., 2018, ApJ, 865, 96
Frewen S. F. N., Hansen B. M. S., 2014, MNRAS, 439, 2442
Gallet F., Bolmont E., Mathis S., Charbonnel C., Amard L., 2017, A&A, 604, A112
Gänsicke B. T., Marsh T. R., Southworth J., Rebassa-Mansergas A., 2006, Science, 314, 1908
Gänsicke B. T., Koester D., Farihi J., Girven J., Parsons S. G., Breedt E., 2012, MNRAS, 424, 333
García-Sánchez J., Weissman P. R., Preston R. A., Jones D. L., Lestrade J.-F., Latham D. W., Stefanik R. P., Paredes J. M., 2001, A&A, 379, 634
Gáspár A., Rieke G. H., 2014, ApJ, 784, 33
Geller A. M., Mathieu R. D., Harris H. C., McClure R. D., 2008, AJ, 135, 2264
Gomes R. S., Fernández J. A., Gallardo T., Brunini A., 2008, The Solar System Beyond Neptune. University of Arizona Press, Arizona, p. 259
Graham J. R., Matthews K., Neugebauer G., Soifer B. T., 1990, ApJ, 357, 216
Grishin E., Veras D., 2019, MNRAS, 489, 168
Grishin E., Perets H. B., Avni Y., 2019, MNRAS, 487, 3324
Gurri P., Veras D., Gänsicke B. T., 2017, MNRAS, 464, 321
Guzik P. et al., 2019, Nat. Astron., 467
Hadjidemetriou J. D., 1963, Icarus, 2, 440
Hamers A. S., Portegies Zwart S. F., 2016, MNRAS, 462, L84
Hamers A. S., Tremaine S., 2017, AJ, 154, 272
Hands T. O., Dehnen W., Gration A., Stadel J., Moore B., 2019, MNRAS, 490, 21
Hao W., Kouwenhoven M. B. N., Spurzem R., 2013, MNRAS, 433, 867
Harrison J. H. D., Bonsor A., Madhusudhan N., 2018, MNRAS, 479, 3814
Hayes W. B., Malykh A. V., Danforth C. M., 2010, MNRAS, 407, 1859
Heisler J., Tremaine S., 1986, Icarus, 65, 13
Hobbs G., Lorimer D. R., Lyne A. G., Kramer M., 2005, MNRAS, 360, 974
Hollands M. A., Koester D., Alekseev V., Herbert E. L., Gänsicke B. T., 2017, MNRAS, 467, 4970
Hollands M. A., Gänsicke B. T., Koester D., 2018, MNRAS, 477, 93
Holsapple K. A., 2007, Icarus, 187, 500
Hurley J. R., Pols O. R., Tout C. A., 2000, MNRAS, 315, 543
Hurley J. R., Tout C. A., Aarseth S. J., Pols O. R., 2001, MNRAS, 323, 630
Jackson A. P., Tamayo D., Hammond N., Ali-Dib M., Rein H., 2018, MNRAS, 478, L49
Jura M., Young E. D., 2014, Annu. Rev. Earth Planet. Sci., 42, 45
Jutzi M., Benz W., Toliou A., Morbidelli A., Brasser R., 2017, A&A, 597, A61
Katz J. I., 2018, MNRAS, 478, L95
Kenyon S. J., Bromley B. C., 2008, ApJS, 179, 451
King I., 1962, AJ, 67, 471
Kobayashi H., Löhne T., 2014, MNRAS, 442, 3266
Koester D., Gänsicke B. T., Farihi J., 2014, A&A, 566, A34
Kokubo E., Yoshinaga K., Makino J., 1998, MNRAS, 297, 1067
Krivov A. V. et al., 2013, ApJ, 772, 32
Krivov A. V., Ide A., Löhne T., Johansen A., Blum J., 2018, MNRAS, 474, 2564
Kroupa P., 2001, MNRAS, 322, 231

Kunitomo M., Ikoma M., Sato B., Katsuta Y., Ida S., 2011, ApJ, 737, 66
Laskar J., Gastineau M., 2009, Nature, 459, 817
Lawler S. M., Shankman C., Kaib N., Bannister M. T., Gladman B., Kavelaars J. J., 2017, AJ, 153, 33
Leão I. C. et al., 2018, A&A, 620, A139
Li D., Mustill A. J., Davies M. B., 2019, MNRAS, 488, 1366
Liou J.-C., Kaufmann D. E., 2008, The Solar System Beyond Neptune. University of Arizona Press, Arizona, p. 425
Löhne T., Krivov A. V., Rodmann J., 2008, ApJ, 673, 1123
Madappatt N., De Marco O., Villaver E., 2016, MNRAS, 463, 1040
Makarov V. V., Veras D., 2019, ApJ, 886, 127
Malamud U., Perets H. B., 2020, MNRAS, 493, 698
Malhotra R., 1993, Nature, 365, 819
Malmberg D., de Angeli F., Davies M. B., Church R. P., Mackey D., Wilkinson M. I., 2007, MNRAS, 378, 1207
Malmberg D., Davies M. B., Heggie D. C., 2011, MNRAS, 411, 859
Mann A. W. et al., 2017, AJ, 153, 64
Manser C. J. et al., 2019, Science, 364, 66
Marois C., Macintosh B., Barman T., Zuckerman B., Song I., Patience J., Lafrenière D., Doyon R., 2008, Science, 322, 1348
Marois C., Zuckerman B., Konopacky Q. M., Macintosh B., Barman T., 2010, Nature, 468, 1080
Martin R. G., Livio M., Smallwood J. L., Chen C., 2020, MNRAS, 494, L17
McGlynn T. A., Chapman R. D., 1989, ApJ, 346, L105
McMillan S., Portegies Zwart S., van Elteren A., Whitehead A., 2012, in Capuzzo-Dolcetta R., Limongi M., Tornambe' A., eds, ASP Conf. Ser. Vol. 453, Advances in Computational Astrophysics: Methods, Tools, and Outcome. Astron. Soc. Pac., San Francisco, p. 129
Meech K. J. et al., 2017, Nature, 552, 378
Mestel L., 1952, MNRAS, 112, 583
Miller R. H., 1964, ApJ, 140, 250
Milone A. P. et al., 2012, A&A, 540, A16
Minchev I., Chiappini C., Martig M., 2013, A&A, 558, A9
Minchev I. et al., 2018, MNRAS, 481, 1645
Moore J. M. et al., 2016, Science, 351, 1284
Morbidelli A., Nesvorny D., 2019, in Prialnik D., Barucci M. A., Young L., eds, The Transneptunian Solar System. Elsevier
Morbidelli A., Tsiganis K., Crida A., Levison H. F., Gomes R., 2007, AJ, 134, 1790
Morbidelli A., Nesvorny D., Laurenz V., Marchi S., Rubie D. C., Elkins-Tanton L., Wieczorek M., Jacobson S., 2018, Icarus, 305, 262
Moro-Martín A., 2018, ApJ, 866, 131
Moro-Martín A., 2019, AJ, 157, 86
Moro-Martín A., Turner E. L., Loeb A., 2009, ApJ, 704, 733
Mustill A. J., Villaver E., 2012, ApJ, 761, 121
Mustill A. J., Marshall J. P., Villaver E., Veras D., Davis P. J., Horner J., Wittenmyer R. A., 2013, MNRAS, 436, 2515
Mustill A. J., Veras D., Villaver E., 2014, MNRAS, 437, 1404
Mustill A. J., Villaver E., Veras D., Gänsicke B. T., Bonsor A., 2018, MNRAS, 476, 3939
Nesvorný D., 2018, ARA&A, 56, 137
Nesvorný D., Morbidelli A., 2012, AJ, 144, 117
Nesvorný D., Vokrouhlický D., 2016, ApJ, 825, 94
Nesvorný D., Vokrouhlický D., Bottke W. F., Noll K., Levison H. F., 2011, AJ, 141, 159
Nesvorný D., Li R., Youdin A. N., Simon J. B., Grundy W. M., 2019, Nat. Astron., 3, 808
Nicholson R. B., Parker R. J., Church R. P., Davies M. B., Fearon N. M., Walton S. R. J., 2019, MNRAS, 485, 4893
Nordhaus J., Spiegel D. S., 2013, MNRAS, 432, 500
Öberg K. I., Wordsworth R., 2019, AJ, 158, 194
Omarov T. B., 1962, Izv. Astrofiz. Inst. Acad. Nauk. KazSSR, 14, 66
'Oumuamua ISSI Team, 2019, Nat. Astron., 3, 594
Parker A. H., 2015, Icarus, 247, 112
Parravano A., McKee C. F., Hollenbach D. J., 2011, ApJ, 726, 27
Pascucci I., Tachibana S., 2010, Protoplanetary Dust: Astrophysical and Cosmochemical Perspectives. Cambridge University Press, Cambridge, p. 263
Pelupessy F. I., van Elteren A., de Vries N., McMillan S. L. W., Drost N., Portegies Zwart S. F., 2013, A&A, 557, A84
Petrovich C., Muñoz D. J., 2017, ApJ, 834, 116
Pfalzner S., Bhandare A., Vincke K., Lacerda P., 2018, ApJ, 863, 45
Pirani S., Johansen A., Bitsch B., Mustill A. J., Turrini D., 2019, A&A, 623, A169
Plummer H. C., 1911, MNRAS, 71, 460
Polishook D., Moskovitz N., Thirouin A., Bosh A., Levine S., Zuluaga C., Tegler S. C., Aharonson O., 2017, Icarus, 297, 126
Portegies Zwart S. F., 2009, ApJ, 696, L13
Portegies Zwart S. F., 2011, Astrophysics Source Code Library, record (ascl:1107.007)
Portegies Zwart S., 2013, MNRAS, 429, L45
Portegies Zwart S., 2019, A&A, 622, A69
Portegies Zwart S. F., Jílková L., 2015, MNRAS, 451, 144
Portegies Zwart S., Torres S., Pelupessy I., Bédorf J., Cai M. X., 2018, MNRAS, 479, L17
Portell de Mora J., García-Berro E., Estepa C., Castañeda J., Clotet M., 2011, in Huang B., Plaza A. J., eds, Proc. SPIE Conf. Ser. Vol. 8183, High-Performance Computing in Remote Sensing. SPIE, Bellingham, p. 818305
Punzo D., Capuzzo-Dolcetta R., Portegies Zwart S., 2014, MNRAS, 444, 2808
Quinlan G. D., Tremaine S., 1992, MNRAS, 259, 505
Rafikov R. R., 2018, ApJ, 861, 35
Raghavan D. et al., 2010, ApJS, 190, 1
Rao S., Meynet G., Eggenberger P., Haemmerlé L., Privitera G., Georgy C., Ekström S., Mordasini C., 2018, A&A, 618, A18
Rappaport S. et al., 2018, MNRAS, 474, 1453
Raymond S. N., Armitage P. J., Veras D., Quintana E. V., Barclay T., 2018a, MNRAS, 476, 3031
Raymond S. N., Armitage P. J., Veras D., 2018b, ApJ, 856, L7
Rein H., Liu S.-F., 2012, A&A, 537, A128
Schröder K.-P., Smith R. C., 2008, MNRAS, 386, 155
Sellwood J. A., Binney J. J., 2002, MNRAS, 336, 785
Shannon A., Dawson R., 2018, MNRAS, 480, 1870
Shannon A., Wu Y., 2011, ApJ, 739, 36
Shannon A., Jackson A. P., Veras D., Wyatt M., 2015, MNRAS, 446, 2059
Shannon A., Jackson A. P., Wyatt M. C., 2019, MNRAS, 485, 5511
Shara M. M., Hurley J. R., Mardling R. A., 2016, ApJ, 816, 59
Sibthorpe B., Kennedy G. M., Wyatt M. C., Lestrade J.-F., Greaves J. S., Matthews B. C., Duchêne G., 2018, MNRAS, 475, 3046
Silsbee K., Tremaine S., 2018, AJ, 155, 75
Smallwood J. L., Martin R. G., Livio M., Lubow S. H., 2018, MNRAS, 480, 57
Smallwood J. L., Martin R. G., Livio M., Veras D., 2019, MNRAS , submitted
Spurzem R., 1999, J. Comput. Appl. Math., 109, 407
Spurzem R., Giersz M., Heggie D. C., Lin D. N. C., 2009, ApJ, 697, 458
Staff J. E., De Marco O., Wood P., Galaviz P., Passy J.-C., 2016, MNRAS, 458, 832
Stern S. A., 1990, PASP, 102, 793
Stern S. A. et al., 2015, Science, 350, aad1815
Stern S. A. et al., 2019, Science, 364, aaw9771
Stone N., Metzger B. D., Loeb A., 2015, MNRAS, 448, 188
Sun M., Arras P., Weinberg N. N., Troup N. W., Majewski S. R., 2018, MNRAS, 481, 4077
Swan A., Farihi J., Wilson T. G., 2019a, MNRAS, 484, L109
Swan A., Farihi J., Koester D., Hollands M., Parsons S., Cauley P. W., Redfield S., Gänsicke B. T., 2019b, MNRAS, 490, 202
Tapamo H., 2009, in Gracia J., de Colle F., Downes T., eds, Lecture Notes in Physics, Vol. 791, Jets From Young Stars V. Springer-Verlag, Berlin, p. 3
Thommes E. W., Duncan M. J., Levison H. F., 2002, AJ, 123, 2862
Tiscareno M. S., Malhotra R., 2009, AJ, 138, 827
Torres S., Cai M. X., Brown A. G. A., Portegies Zwart S., 2019, A&A, 629, A139

Tsiganis K., Gomes R., Morbidelli A., Levison H. F., 2005, Nature, 435, 459
van Elteren A., Portegies Zwart S., Pelupessy I., Cai M. X., McMillan S. L. W., 2019, A&A, 624, A120
Vanderbosch Z. et al., 2019, preprint (arXiv:1908.09839)
Vanderburg A. et al., 2015, Nature, 526, 546
Veras D., 2016a, R. Soc. Open Sci., 3, 150571
Veras D., 2016b, MNRAS, 463, 2958
Veras D., Armitage P. J., 2004, MNRAS, 347, 613
Veras D., Evans N. W., 2013a, MNRAS, 430, 403
Veras D., Evans N. W., 2013b, Celest. Mech. Dyn. Astron., 115, 123
Veras D., Gänsicke B. T., 2015, MNRAS, 447, 1049
Veras D., Moeckel N., 2012, MNRAS, 425, 680
Veras D., Scheeres D. J., 2020, MNRAS, 492, 2437
Veras D., Wyatt M. C., 2012, MNRAS, 421, 2969
Veras D., Wyatt M. C., Mustill A. J., Bonsor A., Eldridge J. J., 2011, MNRAS, 417, 2104
Veras D., Hadjidemetriou J. D., Tout C. A., 2013a, MNRAS, 435, 2416
Veras D., Mustill A. J., Bonsor A., Wyatt M. C., 2013b, MNRAS, 431, 1686
Veras D., Jacobson S. A., Gänsicke B. T., 2014a, MNRAS, 445, 2794
Veras D., Shannon A., Gänsicke B. T., 2014b, MNRAS, 445, 4175
Veras D., Evans N. W., Wyatt M. C., Tout C. A., 2014c, MNRAS, 437, 1127
Veras D., Eggl S., Gänsicke B. T., 2015a, MNRAS, 452, 1945
Veras D., Eggl S., Gänsicke B. T., 2015b, MNRAS, 451, 2814
Veras D., Leinhardt Z. M., Eggl S., Gänsicke B. T., 2015c, MNRAS, 451, 3453
Veras D., Marsh T. M., Gänsicke B. T., 2016a, MNRAS, 461, 1413
Veras D., Mustill A. J., Gänsicke B. T., Redfield S., Georgakarakos N., Bowler A. B., Lloyd M. J. S., 2016b, MNRAS, 458, 3942
Veras D., Carter P. J., Leinhardt Z. M., Gänsicke B. T., 2017a, MNRAS, 465, 1008
Veras D., Georgakarakos N., Dobbs-Dixon I., Gänsicke B. T., 2017b, MNRAS, 465, 2053
Veras D., Georgakarakos N., Gänsicke B. T., Dobbs-Dixon I., 2018, MNRAS, 481, 2180
Veras D., Higuchi A., Ida S., 2019, MNRAS, 485, 708
Veras D., 2020, MNRAS, in press (arXiv:2003.00020)
Veras D., Kurosawa K., 2020, MNRAS, in press (arXiv:2003.01127)
Veras D., McDonald C. H., Makarov V. V., 2020a, MNRAS, 492, 5291
Veras D., Tremblay P.-E., Hermes J. J., McDonald C. H., Kennedy G. M., Meru F., Gänsicke B. T., 2020b, MNRAS, 493, 765
Villaver E., Livio M., Mustill A. J., Siess L., 2014, ApJ, 794, 3
Vokrouhlický D., Bottke W. F., Chesley S. R., Scheeres D. J., Statler T. S., 2015, Asteroids IV. University of Arizona Press, Arizona, p. 509
Volk K., Malhotra R., 2019, AJ, 158, 64
Wang L., Spurzem R., Aarseth S., Nitadori K., Berczik P., Kouwenhoven M. B. N., Naab T., 2015, MNRAS, 450, 4070
Wang L. et al., 2016, MNRAS, 458, 1450
Wang Y.-H., Perna R., Leigh N. W. C., 2020, preprint (arXiv:2002.05727)
Warner B. D., Harris A. W., Pravec P., 2009, Icarus, 202, 134
Weissman P. R., Levison H. F., 1997, ApJ, 488, L133
Welsh B. Y., Montgomery S. L., 2015, Adv. Astron., 2015, 980323
Williams G., 2017, MPEC, 2017-U181: : Comet C/2017 U1 (PanStarrs). IAU Minor Planet Center
Williams J. P., Cieza L. A., 2011, ARA&A, 49, 67
Winter A. J., Clarke C. J., Rosotti G., Ih J., Facchini S., Haworth T. J., 2018, MNRAS, 478, 2700
Wisdom J., Holman M., 1991, AJ, 102, 1528
Wolff S., Dawson R. I., Murray-Clay R. A., 2012, ApJ, 746, 171
Wyatt M. C., Smith R., Su K. Y. L., Rieke G. H., Greaves J. S., Beichman C. A., Bryden G., 2007, ApJ, 663, 365
Wyatt M. C., Farihi J., Pringle J. E., Bonsor A., 2014, MNRAS, 439, 3371
Wyatt M. C., Bonsor A., Jackson A. P., Marino S., Shannon A., 2017, MNRAS, 464, 3385
Xu S., Zuckerman B., Dufour P., Young E. D., Klein B., Jura M., 2017, ApJ, 836, L7
Xu S., Dufour P., Klein B., Melis C., Monson N. N., Zuckerman B., Young E. D., Jura M. A., 2019, AJ, 158, 242
Zakamska N. L., Tremaine S., 2004, AJ, 128, 869
Zeebe R. E., 2015, ApJ, 798, 8
Zheng X., Kouwenhoven M. B. N., Wang L., 2015, MNRAS, 453, 2759
Zotos E. E., Veras D., 2020, submitted
Zuckerman B., Becklin E. E., 1987, Nature, 330, 138
Zuckerman B., Koester D., Reid I. N., Hünsch M., 2003, ApJ, 596, 477
Zuckerman B., Koester D., Melis C., Hansen B. M., Jura M., 2007, ApJ, 671, 872
Zuckerman B., Melis C., Klein B., Koester D., Jura M., 2010, ApJ, 722, 725

This paper has been typeset from a TEX/LATEX file prepared by the author.